EFFECT OF SPIN ON MASS AND RADIUS OF NEUTRON STARS

by

Jorge Calderon Noguez

A thesis submitted in partial fulfillment of the requirements for the degree of

Master of Science

Department of Physics
University of Alberta

Abstract

Neutron stars are some of the densest objects in the Universe, with densities in their cores that are larger than that of the atomic nucleus. Their relatively small size allows them to spin very rapidly, with speeds at the equator that are a large fraction of the speed of light. Being some of the densest objects in existence, it is understandable that we want to know what they are made of. Different proposals have been made leading to various equations to describe the state of matter inside, also known as equation of state (EOS), but there is no conclusive evidence proving that one EOS is correct. In this work, we show simulations for the rotational evolution of various neutron stars from a static state to their maximum spin frequencies for different EOS. We show the fractional increase in mass, M, and radius, R, during the spin-up process of these rapidly rotating objects. We also find quasi-universal relations that depend on the dimensionless quantities of compactness (GM/Rc^2) and the squared value of angular velocity ($\Omega^2 R^3/GM$) that are almost independent of the EOS used.

Preface

This thesis is the original work by Jorge Calderon Noguez, conducted under supervision by Sharon Morsink at the University of Alberta.

Chapters 3, 4, 5 of this thesis consists of a manuscript in preparation, to be submitted to a refereed journal as Calderon Noguez & Morsink, "Effect of spin on mass and radius of neutron stars".

For the work presented in Chapter 3, we modified a code written by Stergioulas & Friedman (1995) to compute sequences of neutron stars, each of them with a constant value of rest mass (mass of all the particles in the star).

Our modifications in the software based on Stergioulas & Friedman (1995) will be available as a public domain code under the name of NSSS (Neutron Stars Spin Sequences). Along with this, we also wrote NSSPlots (Neutron Star Sequences Plots) to show graphs of different physical properties of the sequences computed.

"Study hard what interests you the most in the most undisciplined, irreverent and original manner possible"

Richard P. Feynman

Acknowledgements

This work would not have been possible without the help and guidance of all the people involved. Thank you to my supervisor **Sharon Morsink** for her guidance and encouragement during the program; to my committee members **Gregory Sivakoff**, **Rodrigo Fernandez**, and **Aksel Hallin** for their feedback to improve this thesis; to the **University of Alberta Department of Physics** and the **astrophysics research group** to help me develop different skills for my career; to my **family** and **friends** for all their love, support, and numerous encouragement talks in this journey.

Contents

List of Tables

List of Figures

List of Abbreviations

ATNF	Australian Telescope National Facility
EOS	Equation of State
eXTP	enhanced X-ray Timing and Polarimetry
MSP	Millisecond Pulsar
NICER	Neutron star Interior Composition ExploreR
NS	Neutron Star
NSSPlots	Neutron Star Sequences Plots
NSSS	Neutron Star Spin Sequences
NuSTAR	Nuclear Spectroscopic Telescope Array
ROSAT	ROentgen SATellite
STROBE-X	Spectroscopic Time-Resolving Observatory for Broadband X-rays
XMM	X-ray Multi-Mirror Mission

Chapter 1

Introduction

1.1 Neutron Stars

When a massive star reaches the end of its life, it goes supernova. This powerful explosion pushes the top layers of the star out and, combined with gravitational collapse, the core is compressed to higher than atomic densities. The object left behind is called a neutron star (NS), and it is one of the densest objects in the universe. The first time an object like this was proposed, was by Baade & Zwicky (1934); they thought that a very small and very dense object composed of mostly neutrons must exist. After some years the first computation of such massive compact objects was made by Oppenheimer & Volkoff (1939). Nowadays, when we know for sure that these kind of stars exist, we have found approximately 2700 neutron stars, according to the ATNF pulsar catalogue[1].

Neutron stars (NSs) have been discovered mainly in radio wavelengths. This radiation comes from synchrotron and curvature radiation emitted by accelerated electrons and positrons. These objects are often observed as pulsars, which are NSs that emit radiation from their magnetic poles. The first pulsar was found by Jocelyn Bell, and published by Hewish et al. (1968). Even when the

[1] `https://www.atnf.csiro.au/research/pulsar/psrcat/`

majority of the discoveries were in radio, the first study of a NS observation in X-rays was that of Scorpius X-1, by Shklovsky (1967), who concluded that it was a neutron star undergoing accretion. After this event the discoveries were more frequent, like the discovery of the Crab pulsar in the following year (Comella et al., 1969).

NSs have a typical mass of $M = 1.4\,\mathrm{M}_{\odot}$, a typical radius of $R = 12$ km, and a typical temperature of $T \sim 10^6$ to 10^8 K, which cools as time passes. NSs make several rotations per second (conservation of angular momentum from the original star is one way to impart spin), and when accreting matter from a companion in a binary system, they can be spun up by accretion to spin periods on the order of milliseconds. The fastest known pulsar is PSR J1748-2446, discovered by Hessels et al. (2006). This pulsar has a spin frequency of $\nu = 716.356$ Hz, and is located in the globular cluster Terzan 5. There is another pulsar that, at the time of its discovery in 2007, made people think that it was the fastest spinning pulsar. This pulsar was XTE J1739-285 (Kaaret et al., 2007), with a burst oscillation frequency of $\nu = 1122$ Hz, but there is no evidence that this is the real spin frequency (Chakrabarty, 2008).

It is not known, with precision, the density of neutron star matter, but it is thought that it has values close to $\rho_{\mathrm{ns}} = 2.8 \times 10^{14}$ g/cm^3, which is the nuclear saturation density (density in an atomic nucleus), but in the core densities could potentially be 10 times higher (Pethick et al., 1991).

1.2 The Physics of Neutron Stars

Oppenheimer & Volkoff (1939) hypothesized the existence of a star composed of a neutron gas. To describe it, they assumed, as first approximation, that there is no interaction between all the neutrons in the gas. Nowadays, we know that this cannot happen; in a neutron star there are degenerate neutrons, protons, and relativistic electrons. This mixture occurs at densities above 4×10^{11} g/cm^3.

A gas composed purely of neutrons would be unstable if the electrons are non-degenerate; the neutrons will decay following the β-decay process,

$$n \rightarrow p + e^{-} + \bar{\nu}_e, \tag{1.1}$$

which, as we can see, produces energy. A process that happens inside a neutron star is the inverse β-decay process, in which protons are converted into neutrons, because energy is provided in the form of electrons that move with velocities close to the speed of light (Longair, 2011; Zeldovich & Novikov, 2014)

$$e^{-} + p \rightarrow n + \nu_e. \tag{1.2}$$

This decay process happens when the total energy of the electron exceeds the mass difference between the neutron and the proton,

$$E = \gamma m_e c^2 \geq (m_n - m_p)c^2 = 1.29 \text{ MeV}, \tag{1.3}$$

where m_e, m_n, and m_p are the masses of the electron, the neutron, and the proton, respectively. When the density increases, matter will be composed mainly of neutrons; in a neutron star there are approximately 8 neutrons per proton. The electrons and ions fill up all the free states. Due to this the star maintains a neutral charge. The large ratio of neutrons compared to protons and electrons assures that the neutron degeneracy pressure dominates over the electron degeneracy pressure.

In a neutron star, the neutrons' Fermi momenta is

$$p_F = h \left(\frac{3n}{8\pi} \right)^{1/3}, \tag{1.4}$$

where n is the number density of neutrons. Following on this, the Fermi energy

will be

$$E_F = \left(p_F^2 c^2 + m_n^2 c^4\right)^{1/2}. \tag{1.5}$$

Using equations (1.4) and (1.5) we can find the Fermi energy for a neutron in a NS with a number density of $n = 5.6 \times 10^{37}$ cm^{-3}. We assume that, in equation (1.5), $m_n^2 c^4 = 0$, because degenerate pressure comes from the momentum of the relativistic particles,

$$E_F^n = 237 \text{ MeV}. \tag{1.6}$$

And considering that $T = 10^6$ K, the thermal energy is

$$E_T^n = 8.62 \times 10^{-5} \text{ MeV}. \tag{1.7}$$

Comparing the results (1.6) and (1.7), we can see that the Fermi energy is seven orders of magnitude larger than the thermal energy.

1.3 Evolution of a Neutron Star

When a main sequence star that is $8\,\mathrm{M}_\odot$ or above reaches the end of its life, it becomes a supernova (Bally & Reipurth, 2006). In this high-energy event, a neutron star is formed.

As the progenitor star approaches the supernova stage, the fuel being burnt by nuclear reactions produces iron, which accumulates in the core. Since iron cannot be used to power the star, the thermal pressure will decrease, and the star will not be able to overcome gravitational collapse. Temperature and density increases, and electrons and protons combine via electron capture, producing neutrons and antineutrinos that fly away at speeds close to the speed of light. In this stage, a process called photodissociation occurs, which is the

breakup of iron nuclei into alpha particles by high-energy gamma rays. Density increases until it reaches a value of the order of 10^{14} g/cm^3, which is the average nuclear density ($\rho_{\rm ns}$). At this point, the collapsing outer layers of the star are pushed away by the neutrinos, causing the supernova explosion and leaving behind a NS (Prakash et al., 2001).

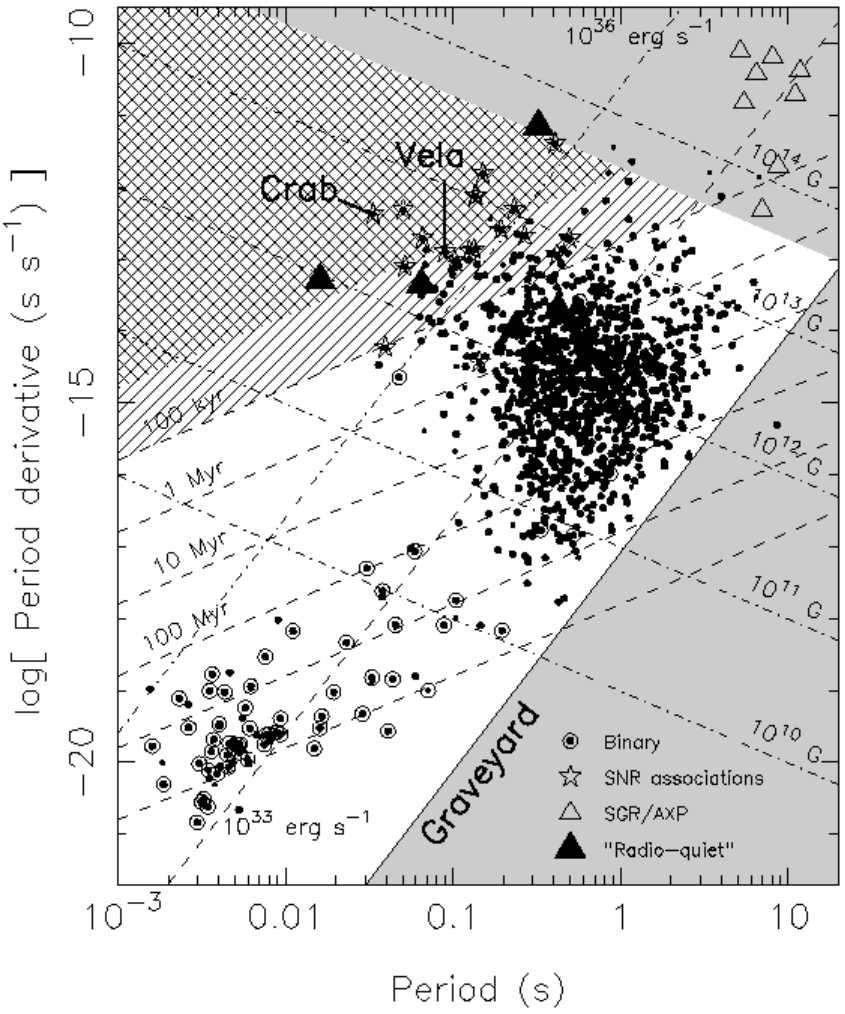

Figure 1.1: $\dot{P}-P$ diagram (Lorimer & Kramer, 2004) that shows the spin down rate as a function of the period of the known pulsars. There are also lines that denote the constant values of characteristic age (in Myrs), magnetic field (in G), and spin down luminosity (in erg s^{-1}).

Approximately one minute after the supernova explosion, the newly created NS becomes transparent to neutrinos. During this state, the cooling of the star

happens in two ways: one is neutrino emission from the entire star; and the other is by the thermal emission from the surface of the star. In the latter process, photons come from the internal structure of the NS, which will stay in this non isothermal state for the first 10–100 years of life. During this period of time and approximately for the next 10^5 years, neutrino emission is the dominant cooling process. After that stage, thermal photon emission dominates. The fact that the cooling process is dominated by neutrino emission does not mean that it is the only mechanism taking place in the neutron star; cooling is also regulated by photon emission, superfluidity of its interior, and by heat insulation in the outer layers due to the presence of lighter elements in the surface (Haensel et al., 2007).

The majority of isolated NSs are observed as radio pulsars. This is because they have a strong magnetic field, and they rotate with a high frequency. A radio pulsar emits a non-thermal multiwavelength magnetospheric radiation and, sometimes, thermal-like radiation from its hot polar caps on the surface, just like the Vela and Geminga pulsars, which have been observed from the infrared to the gamma range (Danilenko et al., 2011).

1.4 Spin Evolution

The spin evolution of NSs can be studied by plotting them on the $\dot{P}-P$ diagram (Haensel et al., 2007), which can be seen in Figure 1.1. In this diagram we see $\dot{P}$ as a function of P. The latter variable, P, is the period of the NS, which is the time that the NS takes to complete one revolution. $\dot{P}$ is the spin down rate, or in other words, it is the rate of change in the period or the time increased per unit time. This will be discussed in subsection 1.4.1.

In Figure 1.1 we can see four populations of pulsars. The NSs found in supernova remnants (SNR) are located in the top (where the Crab and Vela pulsars are labelled). Binary pulsars are made up of a pulsar, and a star or

NS companion, they are located in the lower left part of the diagram. AXP (Anomalous X-ray pulsars) and SGR (Soft Gamma-ray Repeaters) are objects that emit large amounts of gamma and X-ray radiation; they are located at the top right of the diagram, and are believed to be magnetars (young and isolated NSs with large magnetic fields). Radio-quiet objects are NSs that do not seem to emit in radio; they are in the same region in the diagram as the SNR pulsars. The final population are the pulsars represented by a simple dot, they are pulsars that are loosing energy relatively quickly and spin relatively slowly.

Old and slow rotating isolated neutron stars have weak electric fields and therefore produce a weak outflow of particles from their surfaces. This means that their magnetospheric activity is slowly disappearing and, as a result, they have little, or even, no radiation in radio (Haensel et al., 2007). These NSs have large P and small $\dot{P}$ and could be placed in the lower right part of the diagram, where the graveyard is located. The line separating the graveyard from the neutron stars and pulsars is called the *pulsar death line*, which can change depending on the equation of state (Zhou et al., 2017).

Depending on the circumstances of the neutron star, it can decrease or increase its rotational frequency. This is known as spinning-down and spinning-up.

1.4.1 Neutron Star Spin-Down

Let us consider an isolated neutron star. We know that after a supernova the core of the original star collapses to a neutron star, and it spins at high values of frequency. But, as time passes, the rotational kinetic energy will be radiated away by magnetic dipole radiation and eventually, the star will come to a static state. This is the reason why older neutron stars take several seconds for a single revolution. This can be seen in the $\dot{P} - P$ diagram in Figure 1.1, where the slowest pulsars are on the right-hand side (the longer the period, the

Figure 1.2: The Crab nebula, that contains the Crab pulsar (red star in the centre) shown in X-ray (blue) and in the optical spectrum (red). This image combines data from the Chandra X-ray Observatory and the Hubble Space Telescope (Credits: X-ray: NASA/CXC/ASU/J. Hester et al.; Optical: NASA/HST/ASU/J. Hester et al.).

slower the rotation is; the shorter the period, the faster the rotation is).

The dashed lines represent lines of constant characteristic age, τ, spin-down luminosity, $\dot{E}$, and the lines with negative slope represent constant magnetic field, B. Related to these lines, we have magnetic dipole radiation, which extracts energy from a pulsar making them rotate slower.

As the neutron star ages, the emission powered by the rotational kinetic energy will cease (Condon & Ransom, 2016), and the star will no longer be observable. It may seem unbelievable that all the observed luminosity of a neutron star can come from its rotational kinetic energy, but it happens. An example of this is the Crab pulsar (Figure 1.2). The luminosity of the nebula is comparable to the rate that the neutron star is losing rotational kinetic energy.

1.4.2 Neutron Star Spin-Up

As we described in the last subsection, neutron stars can be formed with a large rotational frequency and consequently, an oblate shape, where the equatorial radius is larger than the polar radius. As time passes they usually slow down and become more spherical, but there is an instance in which neutron stars increase their rotational frequency. This can happen because a neutron star is accreting material that is orbiting around it. This material comes from a companion star, which makes the neutron star rotate faster (Ritter & King, 2001), as long as the neutron star and its stellar companion are in a close binary system. The fastest rotating NSs are found in Figure 1.1 in the lower left corner. Those binary systems may have been accreting in the past, which is why they are spinning so fast.

This increment of spin frequency due to a companion star is seen in pulsars like the millisecond X-ray pulsar, XTE J1808-359, which is clearly accreting (Wijnands & van der Klis, 1998).

1.5 Equations of State

An equation of state (EOS) is the relationship between pressure, density and temperature, and it is used to describe how the matter behaves. For NSs we have to consider the relative effects of density and temperature. The average temperature of a NS is 10^6 K, but the thermal energy is approximately 7 orders of magnitude smaller than the Fermi energy (as calculated at the end of Section 1.2). This means that we can neglect temperature, and treat NSs as zero-temperature objects. Therefore, the equation of state for neutron stars describes the pressure as a function only of the density.

The equation of state of matter at high densities is one of the most important properties that are being studied about NSs (Lorimer & Becker, 2009). A possible way to identify the EOS of neutron star is by measuring both the mass

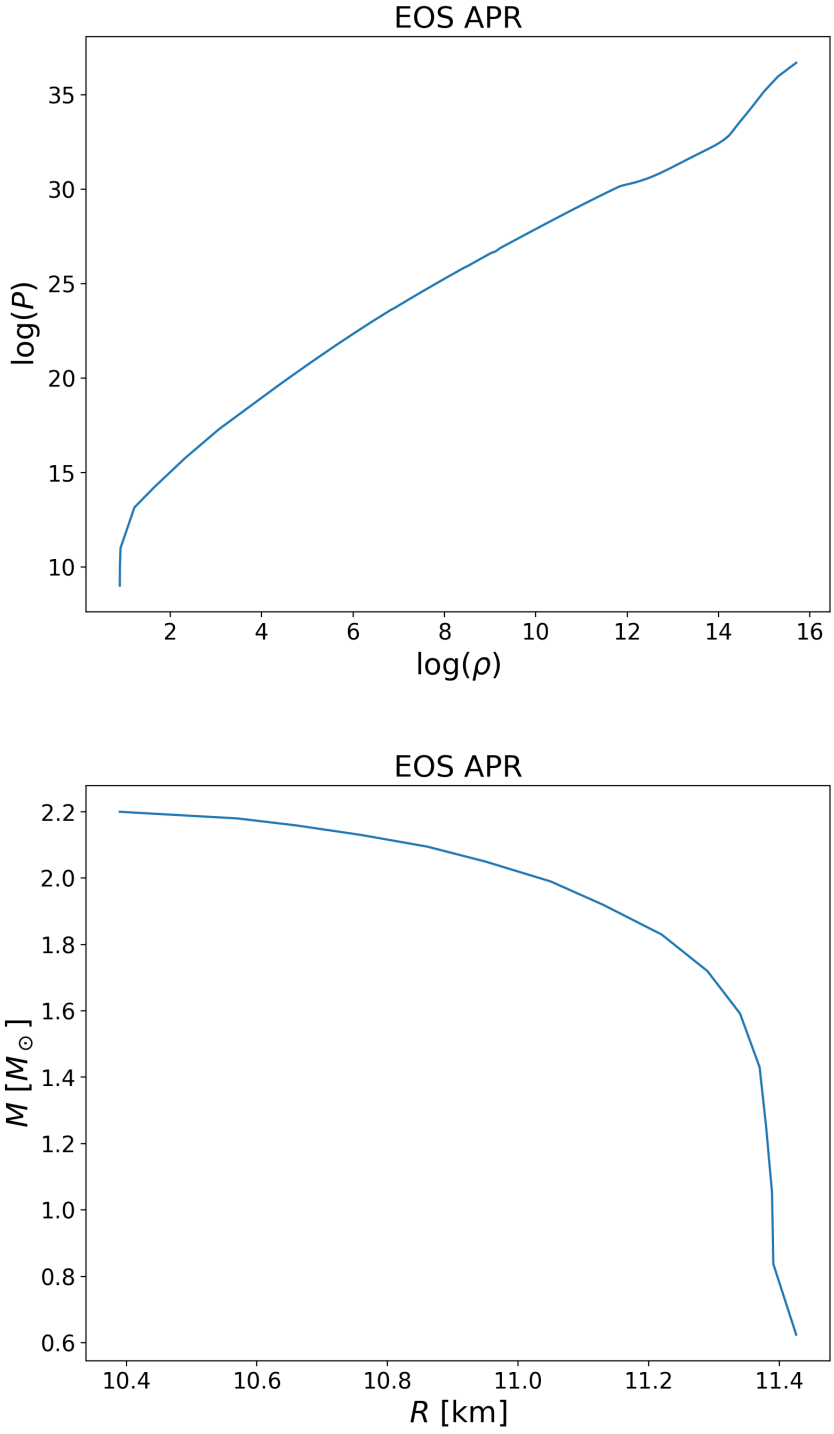

Figure 1.3: Top: Pressure as a function of the density for EOS APR. Bottom: Mass as a function of the equatorial radius of the neutron star for EOS APR. Notice that as the star's radius gets bigger, the less massive it is.

and radius of a neutron star. The Tolman-Oppenheimer-Volkoff (TOV) equations predict a curve of possible masses and radii given an EOS. It would be good news if we only needed one or even two measurements, but we would need to measure several objects in a wide range of masses, probably from $1.0\,\mathrm{M}_\odot$ to more than $2\,\mathrm{M}_\odot$ (Özel & Freire, 2016). Radius is very difficult to measure; if we approximate a neutron star as a pure black body (Lorimer & Becker, 2009), we have that the flux, F, in Newtonian gravity, is given as a function of the distance to the neutron star, D, the surface temperature, T, and the radius, R, so that

$$F = \sigma T^4 \left(\frac{R}{D}\right)^2. \tag{1.8}$$

As we can see, to find the size of a neutron star we need flux, the temperature and the distance. That is why measurements of thermal emission are very important to find the radius, which right now, is still very imprecise.

Mass and radius are dependent on the neutron star's EOS (Ozel & Psaltis, 2009). For example, for EOS APR, we can see their dependence in Figure 1.3; in the top plot we see the pressure increasing along with the density, but it is the opposite for the mass and radius of a NS. In the bottom plot we see that as the star's radius increases, the star's mass is smaller. Both the mass and the radius are dependent on the pressure of the neutron star at densities of $1.85 - 7.4\,\rho_{\mathrm{ns}}$ (Lattimer & Prakash, 2001), where ρ_{ns} is the nuclear saturation density.

There are many proposed EOS because the real one is not known, yet. To make these different EOS, three-body and two-body interactions are considered, as well as other types of forces. There are people who think that there are interacting quarks in the cores of neutron stars (Özel et al., 2010), and others who think that the cores are populated with just neutrons (Page et al., 2011). To find out what the real composition is, we have to wait more time to get

data from future observation projects, like NICER, NuSTAR, or the proposed eXTP and STROBE-X.

1.6 Gravitational Light-Bending

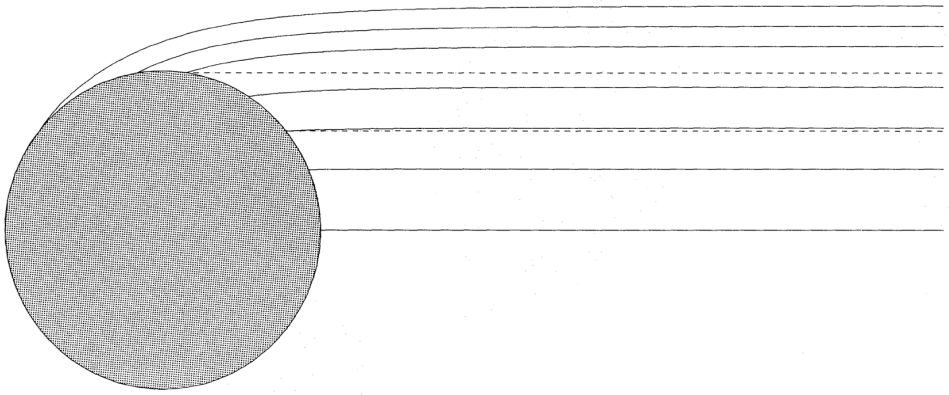

Figure 1.4: Photon paths of a neutron star, which show bending due to effects of general relativity, allowing the observer (located to the right in this figure) to see the hidden part of the neutron star (Nollert et al. (1989)).

A curious property of NSs is that we can see beyond the circular shape that they project (Figure 1.4). Depending on the strength of their gravitational field, we can see a varying amount of the surface behind it. This is due to general relativity, which causes light to travel on curved paths (Kraus, 1998; Nollert et al., 1989). According to general relativity, a massive object will cause spacetime to curve. This effect is described by the Schwarzschild metric, and this curvature will change depending on the object's mass and radius ratio. The curved spacetime will affect the photon's path, which could be bent around the star, orbit the star, fall into it, or escape the star's gravitational well. All of these possibilities make a neutron star look very different compared to how it is in reality. Depending on the paths the photons take, we may see parts in the back of the star, and we could even see the complete surface of the neutron star if the star is small enough.

One way to determine how much the light will be deflected is using the Schwarzschild theory, specifically, using the quotient, R/r_s, where r_s is the Schwarzschild radius given by $r_s = 2GM/c^2$. This is the radius at which we would need to compress an object to make it a black hole, where G is the gravitational constant, M is the mass of the object, and c is the speed of light. The more the ratio decreases, the more surface we can see from the neutron star. This deflection of light helps us determine the X-ray pulse profile of the star (Pechenick et al., 1983; Watts et al., 2016; Sotani & Miyamoto, 2018). To know more about this topic, consult Amason (2019).

Another way to predict how the light will be bent, Sotani & Miyamoto (2018) proposed the use of compactness, which is the quotient of the mass and the radius of the neutron star. For a less compact neutron star, the photons emitted from the back of the star will not be visible to an observer (Pechenick et al., 1983; Watts et al., 2016); but if the star is very compact, the photons will be bent in such a way for the observer to look at the back of the star. This quotient involves the radius of the neutron star, which can be determined if the NS spins rapidly since the Doppler effects are proportional to the radius of the star (Watts et al., 2016).

Due to the strong gravitational field of a neutron star, some of its physical properties change drastically (Potekhin, 2010). The photon frequency, ν_0, in an inertial frame of reference fixed on the neutron star, is redshifted to a frequency of value ν_∞ (the subscript "∞" represents the quantity measured by an observer far from the star), given by

$$z_g = \frac{\nu_0}{\nu_\infty} - 1, \tag{1.9}$$

$$= \left(1 - \frac{2GM}{Rc^2}\right)^{-1/2} - 1. \tag{1.10}$$

Just like the photons' frequencies, the thermal radiation of a star, T_{eff}, is also shifted, in this case to a lower temperature due to relativistic effects; this

perceived temperature by an observer at infinity is

$$T_{eff}^{\infty} = T_{eff}\sqrt{1 - \frac{2GM}{Rc^2}}. \tag{1.11}$$

The photon luminosity of the star, L, measured in its frame of reference will also go through a change caused by the gravitational redshift that is described by

$$L^{\infty} = \left(1 - \frac{2GM}{Rc^2}\right) L, \tag{1.12}$$

so an observer far from the star detects a dimmer star. The previous equation can also be expressed in terms of the apparent radius and the apparent temperature of the neutron star,

$$L^{\infty} \propto R_{\infty}^2 \left(T_{eff}^{\infty}\right)^4. \tag{1.13}$$

The apparent radius, measured by an observer at infinity, appears larger than its real radius, R, due to the gravitational lensing,

$$R_{\infty} = R(1 + z_g). \tag{1.14}$$

This means that both the radius R_{∞}, and the luminosity, L^{∞} agree with the concept of bending of light and the time dilation due to a massive body. This, as we discussed before, allows us to see behind the neutron star. For pulsars, for example, there are instances when both of the polar caps are observed.

1.7 Observations

There were telescopes about 30 to 40 years ago, like EINSTEIN and ROSAT, that had finding NSs in the X-ray range of the electromagnetic spectrum

(Lorimer & Becker, 2009) as one of their goals. Nowadays, there are more advanced telescopes that are being used to focus on the study of NSs. These telescopes are NICER, NuSTAR, Chandra X-ray Observatory, XMM, eXTP and STROBE-X.

NICER (Neutron star Interior Composition ExploreR) was launched in June 2017, allows rotation-resolved spectroscopy of the thermal and non thermal emission of NSs in the soft (0.2-12 keV) X-ray band [2]. This will allow us to uncover the nature of the matter inside a neutron star, dynamic processes, radiation mechanisms, and the threshold of collapse to a black hole (TOV limit). NICER is designed to observe the pulsed emission from X-ray pulsars to indirectly measure the mass and radius with less than 10% uncertainty, as described in the previous section. As a result, we will have a closer idea of what a neutron star interior looks like.

Another telescope is NuSTAR (Nuclear Spectroscopic Telescope Array), launched in June 2012. It observes in the high energy X-rays (3-79 keV)[3] range, which allows NuSTAR to see through dust and gas to study black holes and neutron stars in the Milky Way and other galaxies

Another famous device is the Chandra X-ray Observatory, launched in July 1999. This telescope is designed to observe X-ray[4] emissions from very hot regions of the universe, like supernovae, clusters of galaxies, and matter around neutron stars or black holes.

The observation of thermal flux from neutron stars is very useful nowadays to find the radius of a NS (Heinke et al., 2014). Alongside Chandra, XMM[5] (X-ray Multi-Mirror Mission) also observes the thermal flux from NSs. This mission collects X-rays to determine properties of black holes and even investigate the formation of galaxies.

[2]NASA's HEASARC. `https://heasarc.gsfc.nasa.gov/docs/nicer/`
[3]NuStar website. `https://www.nustar.caltech.edu/page/instrumentation`
[4]Chandra website. `http://chandra.harvard.edu/about/`
[5]XMM website. `http://sci.esa.int/xmm-newton/31249-summary/`

A future project that will shed some light on the unknown properties about neutron stars is eXTP[6] (enhanced X-ray Timing and Polarimetry). Its goals are to find the EOS of matter at super-nuclear density, take measurements of QED effects in magnetized stars, among others.

Another proposed telescope is STROBE-X[7], which will be focusing on X-ray timing and spectroscopy in the 0.2 to 30 keV band. It will provide information on the effects of strong-field general relativity of black holes, as well as their mass and spin. It will also determine the neutron-matter equation by measuring the neutron star's mass-radius relation.

1.8 The Purpose of this Thesis

In this work we analyze how the mass and radius of a NS changes as its rotational frequency increases. Our work considers axial symmetry and solid body rotation. It is based on the numerical methods developed by Komatsu et al. (1989) and Cook et al. (1994).

Each proposed EOS predicts a certain curve of possible mass and radius values if the star is not spinning. However, rotation increases both the mass and radius of a star. So, in reality, each EOS predicts a surface of possible mass, radius and spin values. In this thesis, the relationship between mass, radius, and spin is investigated using the equations of general relativity. As a result, a quasi-universal relation between the fractional increments of mass and radius are found to depend on the dimensionless quantities of compactness (GM/Rc^2), and the squared value of angular velocity ($\Omega^2 R^3/GM$). However, they seem to be independent on the EOS used for the computations.

[6]eXTP website. `https://www.isdc.unige.ch/extp/`
[7]STROBE-X website. `https://gammaray.nsstc.nasa.gov/Strobe-X/index.html`

1.9 Structure of this Thesis

The organization of this thesis is as follows. Chapter 2 involves the mathematical theory to understand neutron stars. Chapter 3 goes over the structure of the code used to compute sequences of rotating neutron stars. Chapter 4 discusses the results found from the analysis of the fractional increase in mass of a rotating NS. Chapter 5 discusses the results that we found when investigating the fractional increase in radius as a NS rotates. Lastly, Chapter 6 summarises the findings of this work. Appendix A has some of the equations computed by the code used here.

Chapter 2

Theoretical Background

In this chapter we are going to discuss the mathematics behind neutron stars and the computation of properties of the same rotating objects. General relativity has to be taken into account when describing neutron stars; the relativity parameter, GM/Rc^2, for a neutron star with a mass of $1.4\,\mathrm{M}_\odot$, and a radius of 12 km, is

$$\begin{aligned}\frac{GM}{Rc^2} &= \frac{(6.67\times10^{-8}\ \mathrm{cm^3 g^{-1} s^{-2}})(1.4\,\mathrm{M}_\odot)}{(12\times10^5\ \mathrm{cm})(2.99\times10^{10}\ \mathrm{cm/s})^2},\\ &= 0.17. \end{aligned} \tag{2.1}$$

Just for comparison, the value of this term for the Earth is $GM_\oplus/R_\oplus c^2 = 13.9\times10^{-10}$. It is nearly zero. This means that the escape velocity is a negligible fraction of the speed of light, c, and equation (2.1) shows that the escape velocity for a NS is a significant amount of c. Therefore the effects of general relativity must be considered in the description of these compact objects. Since the gravitational potential energy contributes to the total mass of the NS, the effective force of gravity has to be stronger.

In Section 2.1 we discuss the metric that describes the region outside of non-rotating neutron stars; this is the Schwarzschild metric. In Section 2.2 we go over some of the physics that are involved in NSs, like the differential

equations that, when integrated, give us the structure of a nonrotating neutron star, also known as, the Tolman-Oppenheimer-Volkoff (TOV) equations. Along with these structure equations we discuss the TOV mass limit for NSs, which is an equivalent to the Chandrasekhar mass for white dwarfs. Finally, in Section 2.3 we go over the equations that are used to compute the physical properties of rotating NSs.

2.1 General Relativity in the Exterior of Spherical Objects

Neutron stars are objects so compact that its escape velocity is a considerable fraction of the speed of light (Wilson, 1974), due to this reason, we have to consider general relativity to describe such massive stars. We begin by assuming spherical symmetry; so we use spherical coordinates (r, θ, ϕ). In a spacetime without gravity, the line element in the Minkowski space is written as (e.g. Schutz, 2009)

$$ds^2 = -c^2dt^2 + dr^2 + r^2\left(d\theta^2 + \sin^2\theta d\phi^2\right). \tag{2.2}$$

This tells us that each surface of constant r and t is a two-dimensional spherical surface (a two-sphere). The distances along curves confined to these surfaces are given when $dt = dr = 0$, then

$$\begin{aligned} dl^2 &= r^2\left(d\theta^2 + \sin^2\theta d\phi^2\right) \\ &= r^2 d\Omega^2. \end{aligned} \tag{2.3}$$

The sphere has a circumference of $2\pi r$ and a surface area of $4\pi r^2$. Any two-surface, where the line element is given by the above equation with r^2 independent of θ and ϕ, has a two-sphere geometry.

Now, the metric for a general static spherically symmetric spacetime with gravity is

$$ds^2 = -e^{2\Phi}c^2dt^2 + e^{2\Lambda}dr^2 + r^2d\Omega^2, \tag{2.4}$$

with $\Phi = \Phi(r)$, and $\Lambda = \Lambda(r)$ (e.g. Schutz, 2009). $\Phi(r)$ is interpreted as the gravitational field in the Newtonian limit, and for Λ, we have

$$e^{2\Lambda} = \left(1 - \frac{2Gm(r)}{rc^2}\right)^{-1}, \tag{2.5}$$

where $m(r)$ is an unknown function, which we will find to be the mass at a position r.

Another thing that has to be taken into account is the source of the gravitational fields in the spacetime in general relativity. The sources are contained in the stress-energy tensor, T (sometimes called stress-energy-momentum tensor). Some of the components are pressure and density, which means they are sources of gravitational fields, and we know that they are related by an equation of state, which, for neutron star matter, have different formulations that are still being tested to find the true EOS.

In general relativity there are also conservation laws, which are involved in the stress-energy tensor. The divergence of this tensor vanishes and we get one equation,

$$(c^2\rho + P)\frac{d\Phi}{dr} = -\frac{dP}{dr}. \tag{2.6}$$

This tells us what pressure gradient is needed to keep the fluid static in the gravitational field inside the star. Now, we need to think how we can describe the exterior of the star. Outside the star there is no matter, so we can safely say that $\rho = P = 0$, which coincidentally, also describe the surface of this spherical

object. Then, we obtain the following set of equations (Schutz, 2009),

$$\frac{dm}{dr} = 0 \quad \text{and} \tag{2.7}$$

$$\frac{d\Phi}{dr} = \frac{mG}{rc^2(r - 2mG/c^2)}. \tag{2.8}$$

When we solve the previous differential equations using the boundary condition $\Phi \to 0$ as $r \to \infty$, we obtain

$$m(r) = M = \text{constant} \quad \text{and} \tag{2.9}$$

$$e^{2\Phi} = 1 - \frac{2GM}{rc^2}, \tag{2.10}$$

which tells us that $m(r)$ is the mass contained in a sphere of radius r, thus M is the total mass of the object. This means that, the metric in the exterior, will be given by the following:

$$ds^2 = \left(1 - \frac{2GM}{rc^2}\right) c^2 dt^2 - \left(1 - \frac{2GM}{rc^2}\right)^{-1} dr^2 - r^2 \left(d\theta^2 + \sin^2\theta d\phi^2\right). \tag{2.11}$$

This is called the Schwarzschild metric. Due to the Birkhoff's theorem, which states that in the vacuum exterior of any spherically symmetric object, the only solution to the Einstein field equations is given by the previous metric (Haardt et al., 2015).

This is the metric that will be used to describe the exterior of a NS. To describe the interior structure we use the Tolman-Oppenheimer-Volkoff (TOV) equations, which are a set of differential equations that can be solved to find more about these compact objects.

2.2 General Relativity in the Interior of Spherical Objects

The TOV equations describe the structure of nonrotating stars. They are the equations of hydrostatic equilibrium for a spherically symmetric body in general relativity (Potekhin, 2010). According to Walecka (2017), to obtain the TOV equations we must assume spherical symmetry, a static situation, and an isotropic fluid with no shear forces, and begin our analysis with the Einstein field equations,

$$G_{\mu\nu} = R_{\mu\nu} - \frac{1}{2} R\, g_{\mu\nu} = \frac{8\pi G}{c^4} T_{\mu\nu}, \tag{2.12}$$

where $R_{\mu\nu}$ is the Ricci curvature tensor, R is the scalar curvature, $g_{\mu\nu}$ is the metric tensor given by the metric in equation (2.2), and $T_{\mu\nu}$ is the stress-energy tensor. The TOV equations are

$$\frac{dP}{dr} = -\frac{Gm(r)\rho(r)}{r^2}\left(1 + \frac{P(r)}{\rho(r)c^2}\right)\left(1 + \frac{4\pi r^3 P(r)}{m(r)c^2}\right)\left(1 - \frac{2m(r)G}{rc^2}\right)^{-1}, \tag{2.13}$$

$$\frac{dm}{dr} = 4\pi r^2 \rho(r) \quad \text{and} \tag{2.14}$$

$$c^2 \frac{d\Phi}{dr} = -\frac{1}{\rho}\frac{dP}{dr}\left(1 + \frac{P(r)}{\rho(r)c^2}\right)^{-1}, \tag{2.15}$$

where Φ is the potential and m is the mass contained in a sphere of radius r. If we integrate equation (2.14) we get the total mass of the star (e.g. Schutz, 2009)

$$M = 4\pi \int_0^R \rho r^2 dr, \tag{2.16}$$

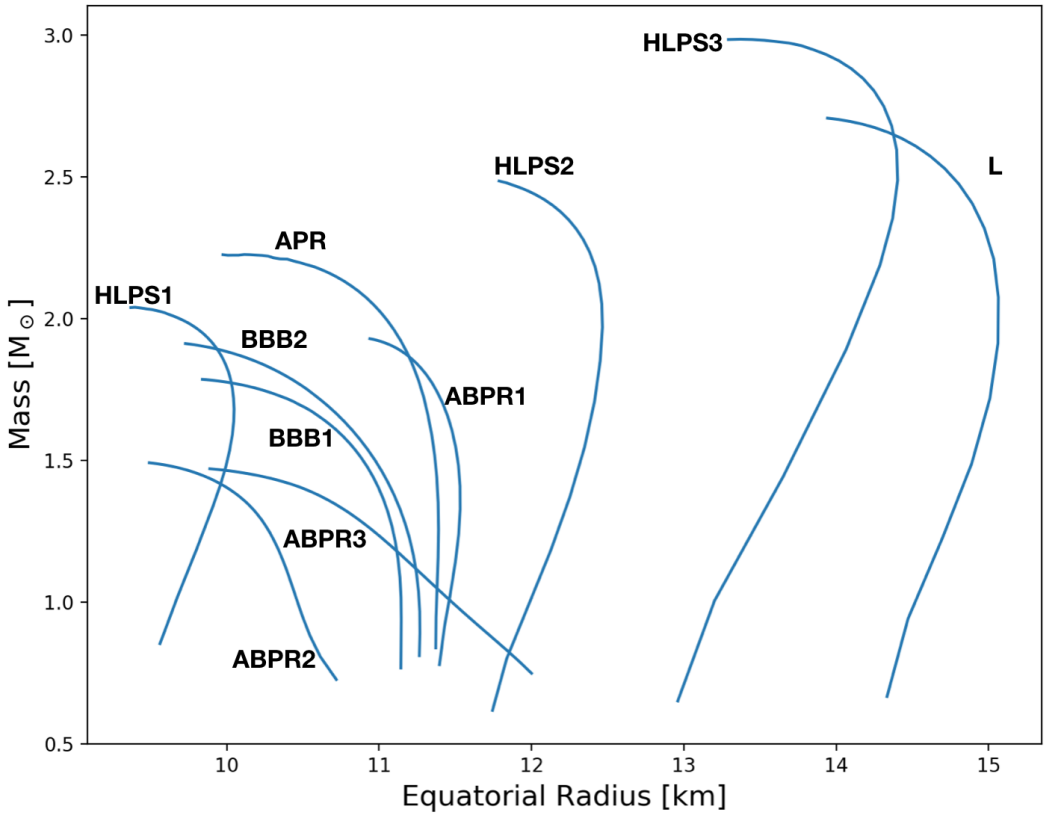

Figure 2.1: Computed relationships between the mass and the radius of non-rotating neutron stars for different equations of state.

while the rest mass is

$$M_0 = 4\pi \int_0^R \frac{\rho r^2}{\sqrt{1 - 2Gm/rc^2}} dr. \tag{2.17}$$

This is the mass of all the particles that make up the neutron star. The TOV equations are used to calculate masses and radii of NSs, so it is understandable that they are also called the equations of structure. To find the relationship between the mass and the radius of a NS (Figure 2.1), they have to be solved numerically (e.g. Lattimer & Prakash, 2004). We computed these relationships for ten different EOS, and considered the stars to be static. In this process we have to take into account some boundary conditions when integrating the TOV equations. We have to assume $P(R) = \rho(R) = 0$, which defines the surface of

the neutron star, which is located at $r = R$. Also, initial values of pressure and density are needed when $r = 0$, these are P_0, and ρ_0, respectively. In the limit of weak gravitational fields, the stellar structure equations reduce to the Newtonian equation for hydrostatic equilibrium and mass conservation.

When we consider the TOV equations, (2.13), (2.14), and (2.15), we can see them as corrections for the Newtonian equations, especially equation (2.13), where the second and third terms in between brackets come from the assumption that pressure is a source of gravity. In other words, pressure is important if P/ρ is large (gas particles are moving with high speeds) and the last term in equation (2.13) comes from the curvature.

2.2.1 Tolman-Oppenheimer-Volkoff (TOV) Limit

We know that the Chandrasekhar limit is the maximum mass that a white dwarf can have, which is $M_{\rm Ch} = 1.4\,{\rm M}_\odot$. White dwarfs by themselves have a mass lower than this value. If the mass increases by mass transfer of some sort, the electron degeneracy pressure in the white dwarf will not be enough to prevent the collapse, and the white dwarf will collapse and possibly explode in a Type Ia supernova. Similarly to the Chandrasekhar limit, the maximum mass for a neutron star is the Tolman-Oppenheimer-Volkoff (TOV) limit, which if surpassed, leads to the inevitable collapse of a neutron star into a black hole. There are also NSs with a rest mass that exceeds the maximum mass of a spherical nonrotating star, they are known as supramassive neutron stars (Cook et al., 1994). The TOV limit depends on the unknown EOS. Theoretically, for a nonrotating NS the limit on the mass is $3.2\,{\rm M}_\odot$ (Rhoades & Ruffini, 1974), and later improved by Hartle (1978). This limit in mass is due to the relativistic particles having a maximum value of energy, because the speed of light is a constant value.

Observations in 2017 of the first occurrence of gravitational waves due to a neutron star binary merger (GW170817) set a potential mass limit, $M \leq$

$2.7\,\mathrm{M}_\odot$ (Abbott et al., 2017; Margalit & Metzger, 2017). This was the mass of one of the neutron stars involved in the collision. Recently, Rezzolla et al. (2018), combining observations of gravitational waves from merging binary systems of NSs, and quasi-universal relations, were able to set lower and upper limits for the TOV mass, $M_{\rm TOV}$,

$$2.01^{+0.04}_{-0.04} \leq \frac{M_{\rm TOV}}{M_\odot} \lesssim 2.16^{+0.17}_{-0.15}. \tag{2.18}$$

There is a way to measure the mass of NSs, known as the Shapiro delay method. In the solar system it is the measurement of time delays between the transmission of radar pulses and the detection of the reflected ones when pointed to a source (Shapiro, 1964). For pulsars, a delay in pulse arrival times due to the curvature of spacetime is observed when a pulsar passes behind its stellar companion. In this year, using this method, the mass of the millisecond pulsar MSP J0740+6620 was measured, $M = 2.14^{+0.10}_{-0.09}\,\mathrm{M}_\odot$ (Cromartie et al., 2019a; Cromartie et al., 2019b). This object clearly falls in the range of the TOV limit. Earlier, this discovery there was another measurement using magnesium triplet lines, the pulsar PSR J2215+5135, which is in a binary system, has a mass of $2.27^{+0.17}_{-0.15}\,\mathrm{M}_\odot$ (Linares et al., 2018). This last method is less accurate than the Shapiro delay, and is likely to have systematic errors. If the latter pulsar is confirmed to have that mass, it could be the most massive one yet, and will modify the TOV limit, and therefore put constraints on the EOS of neutron star matter.

Another constraint on the EOS comes from the rotation of the neutron star (Lattimer & Prakash, 2004). The upper limit in the rotation a neutron star can have is called the Kepler limit, v_K,

$$v_K = \frac{1}{2\pi}\sqrt{\frac{GM}{R^3}}, \tag{2.19}$$

which is the approximation in Newtonian gravity. General relativity gives a

result of similar order of magnitude, but that equation is not so simple. This is also known as the mass-shedding limit, and it depends on the relationship between pressure and density in the interior of the star. This limit is obtained when the velocity of the stellar surface matches the one of a particle orbiting the star just above the surface.

2.3 Computing a Rotating Neutron Star

For this section to be consistent with the sources (Cook et al., 1994; Komatsu et al., 1989), we are going to use a different notation for some parameters, like density. First of all, the metric considered to compute rotating NSs is

$$ds^2 = -e^{\gamma+\rho}dt^2 + e^{2\alpha}\left(dr^2 + r^2 d\theta^2\right) + e^{\gamma-\rho}r^2\sin^2\theta\left(d\phi - \omega dt\right)^2, \qquad (2.20)$$

where ρ, α, γ, and ω are metric potentials, which are a function of r and θ. The field equations used to find the metric potentials are found in the Appendix.

To compute rotating neutron stars, the code (described in detail in Chapter 3) will solve the stellar structure equations for rotation that come from the Einstein field equations using a Green's function method.

The integrals to find the different types of mass, angular momentum, and rotational kinetic energy are written in terms of dimensionless quantities of the radial coordinate, r, the angular velocity of the star, Ω, the rest–energy density,

ρ_0, the energy density, ε, and the pressure, P, given by Cook et al. (1994),

$$\bar{r} = \kappa^{-1/2} r, \tag{2.21}$$

$$\bar{\Omega} = \kappa^{1/2} \frac{1}{c} \Omega, \tag{2.22}$$

$$\bar{\rho}_0 = \kappa \frac{G}{c^2} \rho_0, \tag{2.23}$$

$$\bar{\varepsilon} = \kappa \frac{G}{c^2} \varepsilon, \tag{2.24}$$

$$\bar{P} = \kappa \frac{G}{c^4} P, \tag{2.25}$$

where $\kappa = c^2/(G\epsilon_0)$, with $\epsilon_0 = 10^{15}$ g/cm^3, G is the gravitational constant, and c is the speed of light.

The computation of all the properties is made on a grid (further discussed in Chapter 3) that is in term of the variables μ and s, defined as

$$\mu = \cos\theta \quad \text{and} \tag{2.26}$$

$$s = \frac{\bar{r}}{\bar{r}_e + \bar{r}}, \tag{2.27}$$

where $\bar{r}_e$ is the coordinate radius of the equator, and r and θ meet the conditions $0 \leq r \leq \infty$, and $0 \leq \theta \leq \pi/2$, respectively. The variables s and μ follow $0 \leq s \leq 1$, and $0 \leq \mu \leq 1$. The total mass, M, which is the sum of the mass of all the particles in the star, and the one due to the effects of rotational kinetic energy and gravitational potential energy, is computed as

$$M = \frac{4\pi\kappa^{1/2} c^2 \bar{r}_e^3}{G} \times \int_0^1 \frac{s^2 ds}{(1-s)^4} \int_0^1 d\,\mu e^{2\alpha+\gamma} \left\{ \frac{\bar{\varepsilon} + \bar{P}}{1-v^2} \left[1 + v^2 + \frac{2sv}{1-s} (1-\mu^2)^{1/2} \hat{\omega} e^{-\rho} \right] + \bar{P} \right\}, \tag{2.28}$$

where v is the proper velocity of matter at the equator with respect to a zero angular momentum observer. It is also called gravitational mass in some liter-

ature. The total rest mass of the star, M_0, is

$$M_0 = \frac{4\pi\kappa^{1/2}c^2\bar{r}_e^3}{G}\int_0^1 \frac{s^2 ds}{(1-s)^4}\int_0^1 d\,\mu e^{2\alpha+(\gamma-\rho)/2}\frac{\bar{\rho}_0}{(1-v^2)^{1/2}}. \tag{2.29}$$

This mass is also known as baryonic mass. Both of this types of masses were described, from the relativistic point of view, in Section 2.2. The total angular momentum of the system, J, is

$$J = \frac{4\pi\kappa c^3\bar{r}_e^4}{G}\int_0^1 \frac{s^3 ds}{(1-s)^5}\int_0^1 d\,\mu(1-\mu^2)^{1/2}e^{2\alpha+\gamma-\rho}(\bar{\varepsilon}+\bar{P})\frac{v}{1-v^2}, \tag{2.30}$$

and finally, the total rotational kinetic energy of the system, T, is given by

$$T = \frac{2\pi\kappa^{1/2}c^2\bar{r}_e^3}{G}\int_0^1 \frac{s^3 ds}{(1-s)^5}\int_0^1 d\,\mu(1-\mu^2)^{1/2}e^{2\alpha+\gamma-\rho}(\bar{\varepsilon}+\bar{P})\frac{v\hat{\Omega}}{1-v^2}, \tag{2.31}$$

where $\hat{\Omega} = \bar{r}_e\bar{\Omega}$. We can also notice that the rotational kinetic energy, T, can be simply be obtained as a function of J,

$$T = \frac{1}{2}\frac{\hat{\Omega}}{c\kappa^{1/2}\bar{r}_e}J. \tag{2.32}$$

Considering the equations in this section and the stellar structure equations for rotation, we can compute a series of rotating neutron stars, which will be further explained in the next chapter.

Chapter 3

Computation of Spinning Neutron Stars Sequences

In this chapter we go over the NSSS (Neutron Star Spin Sequences) code and its capabilities. This code, written in C, is based on the work of Stergioulas & Friedman (1995), which computes the structure of a rapidly rotating neutron star and gives us the mass, M, its equatorial radius, R, the orbital frequency, ν (both co-rotating and counter-rotating), of a particle orbiting at the Innermost Stable Circular Orbit (ISCO), and many other properties of rotating neutron stars. We are modelling *normal* sequences, which means that the rotating star is stable to radial perturbations when it is spun to zero spin frequency. Rotating stars that are not stable to radial perturbations when spun down to zero spin are called supramassive (Cook et al., 1994).

The purpose of NSSS is to compute sequences of rigidly rotating NSs, each with a constant value of rest mass. These sequences allow us to trace the change in a NS's properties as it spins down to slower spin rates without losing any matter.

In Section 3.1 we describe how NSSS works based on a grid that represents a quarter of a NS. In the section 3.2 we explain how one NS is computed. In Sections 3.3 and 3.4 we explain the two different types of sequences that this

software can compute: one that finishes when the Kepler limit, ν_K, is reached; and the other that finishes when a spin limit, $\nu_{\max}$, is given. In Section 3.5 we go over an interpolation method used to simulate NSs with the same value of rest mass. In Section 3.6 we show some examples of the output. Lastly, in Section 3.7, we present the physical properties computed for every NS, and some examples of plots obtained with the python code NSSPlots.

3.1 NSSS Code

To compute the structure of rotating NSs this code uses a two dimensional grid. To do this, the spatial coordinates must first be discretized into this grid. Each cell corresponds to a point where the polar angle, radial coordinates, and the corresponding functions depending on them will be evaluated. The discretization will be made in terms of the variables s and μ, which, in each cell of the grid, will be

$$s = \mathrm{SMAX}\frac{\mathrm{i}-1}{\mathrm{SDIV}-1} \quad \text{and} \tag{3.1}$$

$$\mu = \frac{m-1}{\mathrm{MDIV}-1}, \tag{3.2}$$

with SMAX $= 1$, and $\mu = \cos\theta$, such that $0 \leq \theta \leq \pi/2$. SDIV represents the maximum value in i and MDIV is the maximum value in m. An example of how the grid is structured is seen in Figure 3.1. This grid has a resolution of MDIV $\times$ SDIV $= 7 \times 9$. In this figure we can see the axes, which are i and m, both of which follow $0 < i <$ SDIV and $1 < m <$ MDIV, respectively. If $i = 0$, we have $s = 0$ (which represents the centre of the neutron star); if $i =$ SDIV, we have $s =$ SMAX (a point at infinity outside the neutron star). In the case of μ, if $m = 1$ we have $\mu = 0$ (the equator of the neutron star); and if $m =$ MDIV we have $\mu = 1$ (the north pole of the neutron star). These quantities are represented in Figure 3.2. In each bin we have values of physical

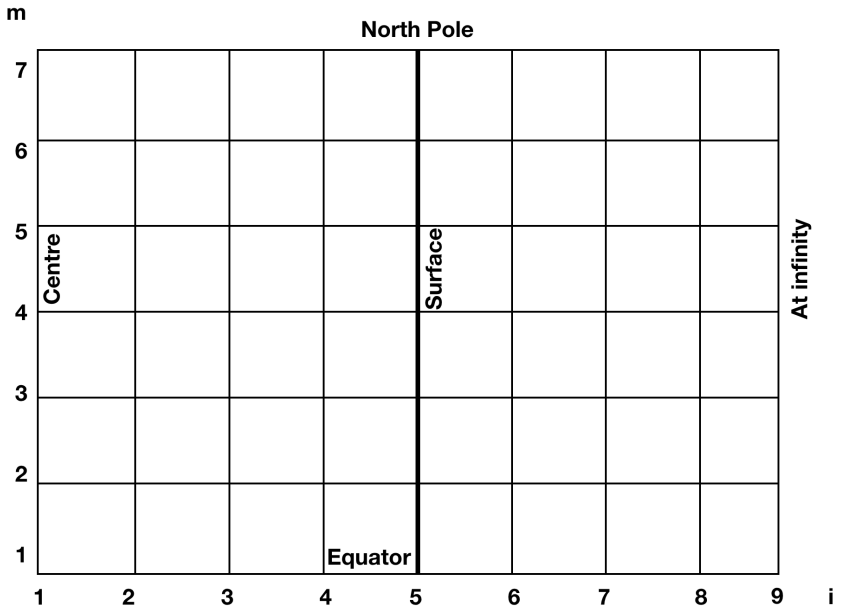

Figure 3.1: Grid that shows how the code is structured. In this case MDIV $\times$ SDIV $= 7 \times 9$.

quantities of the NS, such as the total mass, M, the rest mass, M_0, the angular momentum, J, and the rotational kinetic energy, T. All of which were defined in Section 2.3.

The default grid size of NSSS is MDIV $\times$ SDIV $= 151 \times 301$ (this can be changed in the file *makefile*). The higher the resolution of this grid is, the more accurate the results will be, but also the more time consuming it will be. After each modification in *makefile* the object files (with ".o" extension) have to be deleted. NSSS is able to compute the following:

- One neutron star with a certain value of oblateness;
- Sequences of neutron stars with constant rest mass (mass of the particles that make up the star, denoted by M_0) by increasing the rotational frequency from zero to the limiting spin frequency, ν_K (Kepler limit); and
- Sequences of neutron stars, each with constant M_0, by increasing the rotational frequency from zero to a maximum frequency, $\nu_{\max}$, given by the user.

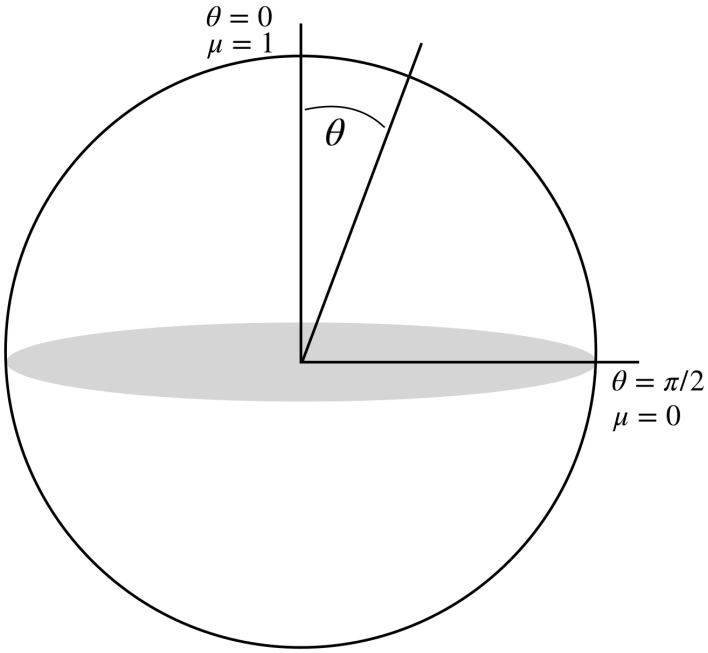

Figure 3.2: Section of a NS where the computation of the data in the star takes place, which is the region from $\theta = 0$ to $\theta = \pi/2$. The equatorial radius of the NS is along the horizontal line and the spin axis goes along the vertical line.

These tasks will be further discussed in Sections 3.2, 3.3, and 3.4. The input parameters that are needed to compute the different tasks are in Table 3.1.

Table 3.1: Input parameters to run NSSS.

Parameter	Description
-f	Name of the file with the tabulated equation of state (EOS)
-e	Central energy density, ε_c (in g/cm^3)
-n	Number of sequences to be produced
-m	Central energy density for the maximum-mass NS for a given EOS, $\varepsilon_{c,M}$
-r	Ratio of r_p/r_e (between 0 and 1)
-t	Maximum spin frequency, $\nu_{\max}$ (in Hz)

To compute the neutron stars we make use of the five different classes of equations of state: ABPR, APR, BBB, HLPS, and L. The first one on the list, ABPR, proposed by Alford, Braby, Paris, & Reddy (2005), describes nuclear and quark matter. There are three versions of it. The EOS APR (Akmal, Pandharipande, & Ravenhall, 1998) describes matter made up of neutrons,

protons, and leptons at zero temperature in its lowest energy state considering two-nucleon (NN) interaction. The EOS BBB proposed by Baldo, Burgio, & Bombaci (1996) describes asymmetric nuclear matter. There are two versions of this equation (BBB1 and BBB2); they also consider NN interactions. The EOS HLPS was presented by Hebeler, Lattimer, Pethick, & Schwenk (2013). It is based on NN and 3N (three nucleons) interactions for microscopic neutron matter. There are three versions of this EOS. The last EOS considered in this work, L, describes the matter as a solid pion, π^0, condensate (Pandharipande et al. (1976), and Pandharipande & Smith (1975)), which is a superfluid formed by these pions that, most of the times, decay into gamma rays.

In NSSS we follow the spin-down of a NS from the maximum spin rate to zero spin without losing or gaining matter. However, computationally speaking, spinning up the star is more helpful to find the rotational limit these objects have. To analyse the data obtained from NSSS we use the python code NSSPlots (Neutron Star Sequences Plots). The plotted data are the physical properties of rotating NSs. These properties can be seen in Table 3.3 in Section 3.7, and are also some of the ones considered in the analysis of NS sequences done by Cook et al. (1994).

3.2 Computing One Neutron Star

To compute a single neutron star we need a tabulated equation of state, a value of the central energy density, ε_c, and the value of the ratio of the polar radius and the equatorial radius, r_p/r_e, which tells us how oblate the neutron star is (Figure 3.3). This quotient is indicative of how fast the neutron star is spinning. The faster it rotates, the more oblate it becomes. For example, when we have a ratio of $r_p/r_e = 1$ the neutron star is spherical and not spinning. The EOS and the central energy density will be used to create a zero-spin neutron star with a certain mass and radius. Then, the quotient r_p/r_e, will be used to

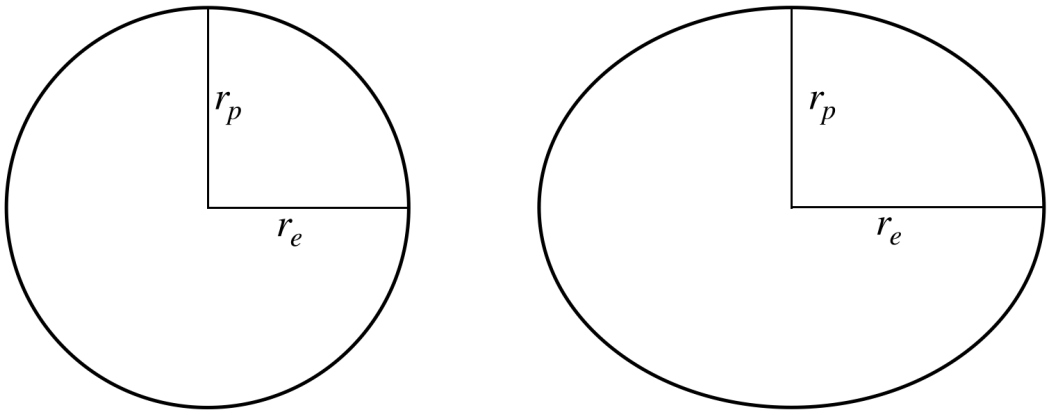

Figure 3.3: Left: Model of a nonrotating neutron star with the two radii considered in NSSS, the equatorial radius, r_e, and the polar radius, r_p. In this case, they are equal to each other. Right: Rapidly rotating neutron star, where now $r_e > r_p$, because of the rotation.

make the star oblate, and therefore, spinning, which will change its equatorial radius and the total mass, since it will gain mass due to the rotational kinetic energy. An example of the command line used to compute a single NS would be

./nsss -f *filename* -e 1.6e15 -r 0.9

The word *filename* is the name of the EOS file (the ten different EOS used can be found in Table 3.2), "-e 1.6e15" indicates that the central energy density at which we begin to computer the first sequence is $1.6 \times 10^{15}\,\mathrm{g/cm^3}$. The "-r 0.9" indicates the value of r_p/r_e.

3.3 Computing Sequences from Zero Spin to the Kepler Limit

The sequences that are computed in this part contain neutron stars that are being spun up until they reach the Kepler limit. The condition is that the NSs that make up one sequence must have the same value of rest mass (also called

baryonic mass). In other words, no matter is being added to the NS and no matter is lost; the mass of the particles that make up the star is kept constant.

Similar to the computation of only one NS, to compute a sequence of neutron stars we need to have a value of ε_c, a tabulated EOS, and the value of the central energy density at which we get the maximum-mass neutron star for each EOS, $\varepsilon_{c,M}$. We computed this last value and its corresponding mass, M_M, rest mass, $M_{0,M}$, and radius R_M. They can be found in Table 3.3.

Table 3.2: Data corresponding to the value of R, r_p/r_e, and ε_c when $M \sim 1\,\mathrm{M}_\odot$ for each EOS considered here (this is one combination). It also shows the value that ε_c has to have when a nonrotating NS with the maximum mass, M_M, is computed; the corresponding values of radius and rest mass are R_M, and $M_{0,M}$, respectively.

	R and ε_c when $M \sim 1\,\mathrm{M}_\odot$				ε_c when M_M is obtained			
EOS	M ($\mathrm{M}_\odot$)	R (km)	r_p/r_e	ε_c (g/cm^3)$\times 10^{15}$	M_M ($\mathrm{M}_\odot$)	$M_{0,M}$ ($\mathrm{M}_\odot$)	R_M (km)	$\varepsilon_{c,M}$ (g/cm^3)$\times 10^{15}$
ABPR1	1.009	11.48288	0.996	0.739545	1.93468	2.26467	10.8059	2.3317
ABPR2	1.004	10.49412	0.994	1.09338	1.49662	1.69859	9.28537	3.3454
ABPR3	1.004	11.57512	0.984	0.983153	1.47598	1.65273	9.67557	3.1508
APR	1.000	11.38782	0.998	0.775	2.23685	2.71921	9.89745	2.8437
BBB1	1.000	11.21119	0.988	0.836243	1.78951	2.08233	9.6527	3.07827
BBB2	1.000	12.09300	0.872	0.777099	1.91853	2.26798	9.48855	3.7733
HLPS1	1.003	9.68367	0.996	1.04467	2.0423	2.51353	9.23051	3.1781
HLPS2	1.000	14.48549	0.706	0.5598	2.49576	3.05768	11.5378	1.9929
HLPS3	1.005	13.21363	0.998	0.449864	2.98219	3.7009	13.3676	1.455
L	1.000	15.18746	0.914	0.352224	2.71085	3.22955	13.7477	1.44216

First of all, to create a sequence of NSs, a nonrotating spherical NS is created. This is going to be the first star in the sequence, and will have a central energy density of $\varepsilon_{c,1}$, and a rest mass of M_0^*. We make sure to store this value of rest mass, because it will be needed to find the stars that continue the sequence.

Now, we need more stars with the same M_0 as the static one, but these stars will rotate gradually faster until one of them reaches the Kepler limit, where the NS gets destroyed due to its rapid rotational frequency. To do this, the

value of r_p/r_e, originally equal to one, is decreased, and three neutron stars are computed, each with this same ratio, but with the following values of central energy density, $\varepsilon_{c,1}$, $\varepsilon_{c,2}$, and $\varepsilon_{c,3}$, such that $\varepsilon_{c,3} < \varepsilon_{c,2} < \varepsilon_{c,1}$. These NSs will have rest masses $M_{0,1}$, $M_{0,2}$, and $M_{0,3}$, such that $M_{0,3} < M_{0,2} < M_{0,1}$. We can notice that $M_{0,1}$ will not be exactly equal to M_0^* because the NS is now rotating.

To find a NS with a rest mass equal to M_0^*, the code makes use of the 3-point interpolation method (described in Section 3.5) to find a value of $\hat{\varepsilon}_c$ such that

$$\varepsilon_{c,3} < \hat{\varepsilon}_c < \varepsilon_{c,1}. \tag{3.3}$$

This value will guarantee the creation of a rotating NS with $M_0 = M_0^*$. Then, using $\hat{\varepsilon}_c$ and a smaller value of r_p/r_e, the second NS in the sequence is created, which will have $\varepsilon_c = \hat{\varepsilon}_c$ and $M_0 = M_0^*$.

This process goes on and r_p/r_e is made smaller (the NS rotates faster) for each computation of one NS, and it continues until the star reaches the Kepler limit, which is the maximum rotational frequency that the star can rotate at. At this point one sequence of neutron stars with constant value of rest mass, M_0^*, is obtained.

To compute another sequence ε_c is increased and the code computes another set of stars in the same way, starting with $r_p/r_e = 1$. This task of computing sequences continues until the total mass, M, of the nonrotating NS is equal to the maximum mass of a nonrotating NS for the given EOS, M_M. Another way to stop the process is by including a parameter (-n) that tells the code to compute only a certain number of sequences. An example of a command line to compute 10 sequences would be

./nsss -f *filename* -e 1.6e15 -n 10 -m 2.3327

filename can be replaced with the file of the chosen EOS (Table 3.2), "-e 1.6e15"

represents the value of ε_c, "-n 10" tells NSSS to compute 10 sequences, and "-m 2.3327" is the value of $\varepsilon_{c,M}$ (notice that we do not need to represent it in scientific notation like ε_c). This last value is needed to compute the maximum-mass NS for each EOS to later be able to normalize some properties.

3.4 Computing Sequences up to a Given Value of Spin Frequency

This task is very similar to the one described in the previous section. The difference is that, in this case, the maximum rotational frequency is not the Kepler limit. It can be set by the user, no matter which EOS is being used. We need a tabulated EOS, a value of ε_c, the value of $\varepsilon_{c,M}$ at which the maximum-mass neutron star is obtained, and one parameter that tells NSSS to compute NSs up to a certain spin frequency, $\nu_{\max}$. The value of $\nu_{\max}$ has to be given in Hz. An example of the command line of initialization for this task is

./nsss -f *filename* -e 1.6e15 -n 10 -m 2.3317 -t 800

This line is the same that was used in the previous section, we just added "-t 800", which tells the code to only compute sequences of neutron stars that rotate with a frequency less than $\nu_{\max} = 800$ Hz.

3.5 3-point Interpolation in NSSS

When computing a sequence of neutron stars, we use the 3-point interpolation method to find a star that can continue the sequence with the same value of rest mass as the initial neutron star in the sequence, that is, $M_0 = M_0^*$. The difference is that the new computed star has a larger ν, and a smaller ε_c, which will be found using this method.

The interpolation function takes three NSs computed with the same value

of r_p/r_e and close values of central energy density, $\varepsilon_{c,1}$, $\varepsilon_{c,2}$, and $\varepsilon_{c,3}$, such that $\varepsilon_{c,3} < \varepsilon_{c,2} < \varepsilon_{c,1}$. The rest masses of the corresponding NSs are $M_{0,1}$, $M_{0,2}$, and $M_{0,3}$, such that $M_{0,3} < M_{0,2} < M_{0,1}$. A graphical representation of this method shows the three stars with these values in Figure 3.4.

The equation of interpolation will be given by

$$0 = a(\varepsilon_c - \varepsilon_{c,2})(\varepsilon_c - \varepsilon_{c,3}) + b(\varepsilon_c - \varepsilon_{c,1})(\varepsilon_c - \varepsilon_{c,3}) + c(\varepsilon_c - \varepsilon_{c,1})(\varepsilon_c - \varepsilon_{c,2}), \tag{3.4}$$

with a, b, and c given by the following equations:

$$a = \frac{y_1}{(\varepsilon_{c,1} - \varepsilon_{c,2})(\varepsilon_{c,1} - \varepsilon_{c,3})}; \tag{3.5}$$

$$b = \frac{y_2}{(\varepsilon_{c,2} - \varepsilon_{c,1})(\varepsilon_{c,2} - \varepsilon_{c,3})}; \tag{3.6}$$

$$c = \frac{y_3}{(\varepsilon_{c,3} - \varepsilon_{c,1})(\varepsilon_{c,3} - \varepsilon_{c,2})}, \tag{3.7}$$

with

$$y_1 = M_0^* - M_{0,1}, \tag{3.8}$$

$$y_2 = M_0^* - M_{0,2}, \quad \text{and} \tag{3.9}$$

$$y_3 = M_0^* - M_{0,3}, \tag{3.10}$$

Rewriting equation 3.4 we have

$$\begin{aligned} a(\varepsilon_{c,2} - \varepsilon_{c,3}\varepsilon_c - \varepsilon_{c,2}\varepsilon_c + \varepsilon_{c,2}\varepsilon_{c,3}) + b(\varepsilon_c^2 - \varepsilon_{c,3}\varepsilon_c - \varepsilon_{c,1}\varepsilon_c + \varepsilon_{c,1}\varepsilon_{c,3}) + \\ c(\varepsilon_c^2 - \varepsilon_{c,2}\varepsilon_c - \varepsilon_{c,1}\varepsilon_c + \varepsilon_{c,1}\varepsilon_{c,2}) = 0, \\ (a+b+c)\varepsilon_c^2 - (a\varepsilon_{c,3} + a\varepsilon_{c,2} + b\varepsilon_{c,3} + b\varepsilon_{c,1} + c\varepsilon_{c,2} + c\varepsilon_{c,1})\varepsilon_c + \\ a\varepsilon_{c,2}\varepsilon_{c,3} + b\varepsilon_{c,1}\varepsilon_{c,3} + c\varepsilon_{c,1}\varepsilon_{c,2} = 0. \end{aligned} \tag{3.11}$$

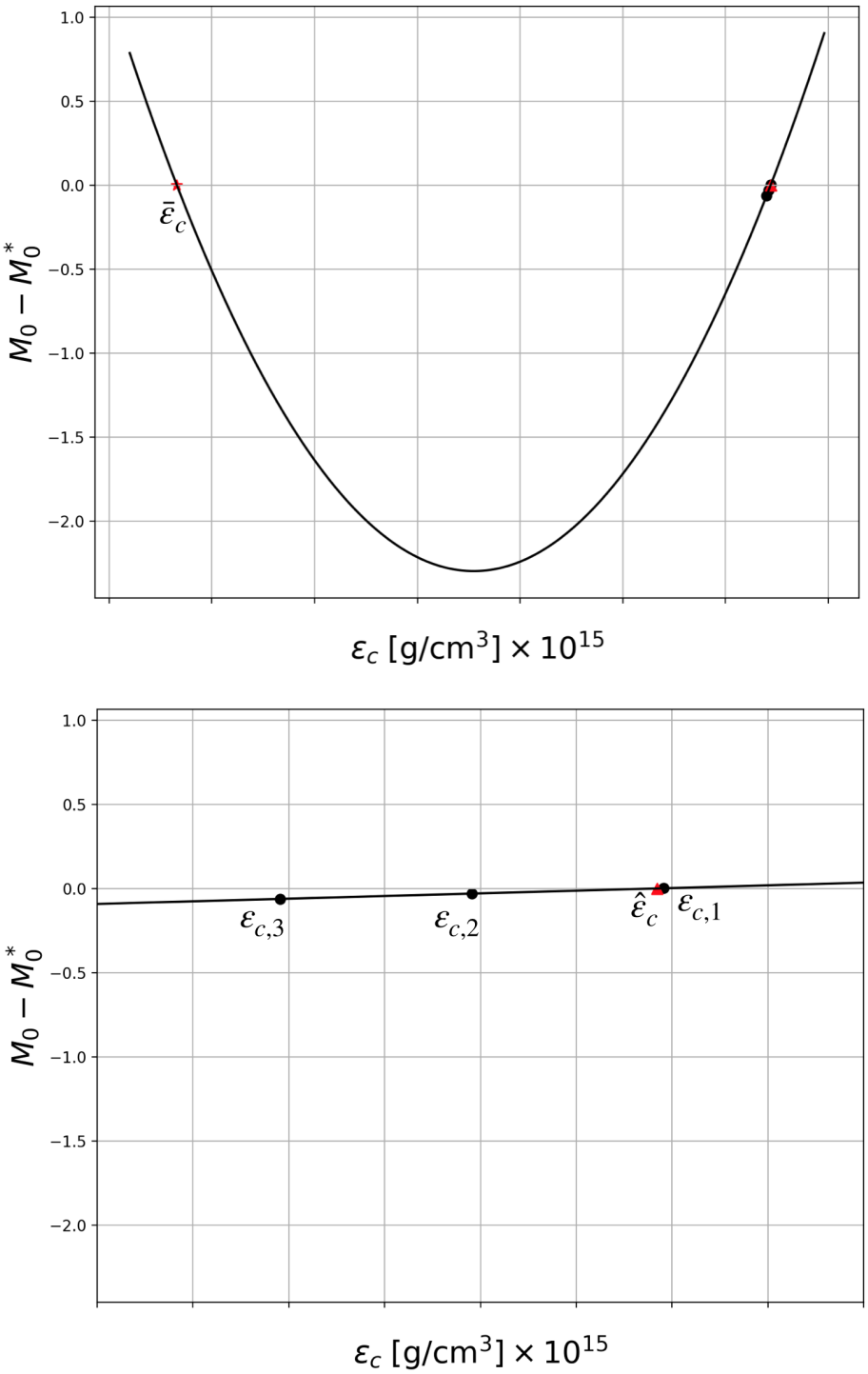

Figure 3.4: Top: Example of the 3 point interpolation method. Notice that on the left side one solution is $\bar{\varepsilon}_c$, which is outside the range of the 3 values of ε_c. Bottom: A closeup of the right side of the plot, where the points are very close together. The solution, $\hat{\varepsilon}_c$ (red triangle), is in between the three values of ε_c.

Notice that the equation is quadratic,

$$(a+b+c)\varepsilon_c^2 - A\varepsilon_c + B = 0, \tag{3.12}$$

with A and B being

$$A = a\varepsilon_{c,3} + a\varepsilon_{c,2} + b\varepsilon_{c,3} + b\varepsilon_{c,1} + c\varepsilon_{c,2} + c\varepsilon_{c,1} \quad \text{and} \tag{3.13}$$

$$B = a\varepsilon_{c,2}\varepsilon_{c,3} + b\varepsilon_{c,1}\varepsilon_{c,3} + c\varepsilon_{c,1}\varepsilon_{c,2}. \tag{3.14}$$

To find the two values of ε_c we simply use the quadratic formula,

$$\varepsilon_c = \frac{A \pm \sqrt{A^2 - 4(a+b+c)(B)}}{2(a+b+c)}. \tag{3.15}$$

The three neutron stars with $\varepsilon_{c,1}$, $\varepsilon_{c,2}$, and $\varepsilon_{c,3}$ can be found in Figure 3.4, along with the two solutions, $\bar{\varepsilon}_c$ and $\hat{\varepsilon}_c$. Notice that only the latter is considered to continue the computation of the following NS, because it falls in the range of $\varepsilon_{c,3} < \hat{\varepsilon}_c < \varepsilon_{c,1}$.

3.6 Output

Let us see some examples of output data from NSSS. First, consider the following command line

```
./nsss -f eos-master/eosL -e 0.36e15 -n 5 -m 1.44216 -t 800
```

This command will take the tabulated L equation of state, that is located in the folder "eos-master", it will also take a starting value of the central energy density, $\varepsilon_c = 0.36 \times 10^{15}$ g/cm^3; the "-n" parameter tells NSSS to compute 5 sequences of NSs, each with a constant M_0. The next command, "-m 1.44216" tells NSSS to compute the nonrotating neutron star with the highest mass for the L equation, which happens at $\varepsilon_{c,M} = 1.44216 \times 10^{15}$ g/cm^3. The last

parameter tells the code that the sequences will finish when the NSs reach $\nu_{\max} = 800$ Hz. Therefore, this line will output the following

Computing star with spin frequency from 0 to 800 Hz

e_c	Mass	Mass_0	StatM	Radius	R-ratio	StatR	Spin	K freq
e15	Msun	Msun	Msun	km	–	km	Hz	Hz
Energy center = 0.36								
0.36	0.99737	1.04661	0.99737	14.51368	1.000	14.51368	0.000	1047.09802
0.35978	0.99738	1.04661	0.99737	14.52606	0.998	14.51368	52.552	1044.55302
0.359603	0.99743	1.04662	0.99737	14.54023	0.996	14.51368	76.061	1042.68951
⋮	⋮	⋮	⋮	⋮	⋮	⋮	⋮	⋮

In the headings, "e_c" is ε_c, "Mass_0" is M_0, "R-ratio" is r_p/r_e, "StatM" is the mass of the first nonrotating NS in each sequence, and it has a radius given by "StatR", "Spin" is the spin frequency, and "K freq" is the Kepler frequency. Notice that the statement before the headings tells us that the NSSS code is computing the sequences up to $\nu_{\max} = 800$ Hz. Even if not all of the physical properties of the neutron star are displayed (see Table 3.3), all of them will be in the output file.

To compute the sequences up to the maximum spin frequency we just omit the command "-t 800", and now the statement above the headings will be "Computing sequences with spin frequency from 0 Hz to the Kepler limit".

Now, let us see how the input and output will be if we compute one neutron star. An example of this would be the following line of commands

```
./nsss -f eos-master/eosL -e 0.36e15 -r 0.9
```

Similar to the last example, this command uses the tabulated equation of state L, the NS will have a central energy density of $\varepsilon_c = 0.36 \times 10^{15}$ g/cm^3 and it will have a ratio of the polar and the equatorial radii of $r_p/r_e = 0.9$, which tells us that the neutron star is rotating. The output is the following set of data that belongs to this one star, which like the previous case, it is denoted by a sentence before the headings:

Computing one neutron star

e_c	Mass	Mass_0	Radius	R-ratio	Spin	K freq
e15	Msun	Msun	km	–	Hz	Hz
0.36	1.05561	1.10903	15.34503	0.900	384.982	995.61897

3.7 Properties Obtained from NSSS

The physical properties of each NS that NSSS outputs are seen in Table 3.3. Note that these are some of the parameters used by Cook et al. (1994) to do a similar analysis of NS sequences.

Table 3.3: Physical properties obtained from NSSS for every single NS computed.

Parameter	Description
ε_c	Central energy density
M	Total mass (in $M_\odot$)
M_0	Rest mass, also known as baryonic mass (in $M_\odot$)
M_*	Mass of the first nonrotating NS in a sequence (in $M_\odot$)
M_M	Maximum mass of a nonrotating NS for a given EOS (in $M_\odot$)
R	Equatorial radius of the NS (in km)
r_p/r_e	Ratio of the polar radius and the equatorial radius
R_*	Equatorial radius of the first nonrotating NS in a sequence (in km)
ν	Rotational frequency (in Hz)
ν_K	Kepler limit for rotation (in Hz)
J	Angular momentum (in cm^2g/s)
T	Rotational kinetic energy (in g)
U	Gravitational binding energy (in g)
R_M	Radius of the maximum-mass NS for a given EOS (in km)
M_M/R_M	Compactness of the nonrotating maximum-mass NS for a given EOS

To analyse the physical properties we make use of various different plots. For some of them, we consider dimensionless or normalized quantities. This is because the behaviour of some of the data can be seen better when it depends only on dimensionless variables. The dimensionless angular velocity can be

calculated in the following manner:

$$\Omega \left(\frac{R^3}{GM} \right)^{1/2}, \tag{3.16}$$

where G is the gravitational constant; M and R are the already known mass and equatorial radius. The compactness is given by

$$\zeta = \frac{GM}{Rc^2}, \tag{3.17}$$

where c is the speed of light. A way to normalize the previous quantity is by dividing it by the maximum compactness, which is the one corresponding to the maximum-mass NS for a given EOS. Its mass and radius are M_M, and R_M. The latter is the radius of the maximum-mass NS, not the maximum radius. Thus the normalization will be

$$\frac{\zeta}{\zeta_{\max}} = \frac{M/R}{M_M/R_M}. \tag{3.18}$$

The Kerr spin parameter can be obtained as well,

$$a = \frac{cJ}{GM}, \tag{3.19}$$

where J is the angular momentum. The normalized version of this parameter is

$$\frac{a}{M} = \frac{cJ}{GM^2}, \tag{3.20}$$

which obeys $0 \leq a/M \leq 1$. The fraction of mass that comes from relativistic sources compared with the rest mass is given by

$$\frac{M - M_0}{M_0}. \tag{3.21}$$

The fractional increase of M compared to the mass of the nonrotating neutron star in the beginning of each sequence is

$$\frac{M - M_*}{M_*}, \tag{3.22}$$

where we keep in mind that M_0 is the same in each sequence. Similarly to the above relation, the fractional increase of the equatorial radius compared to the radius of the nonrotating NS in the beginning of the sequences, is

$$\frac{R - R_*}{R_*}, \tag{3.23}$$

We can see in Figures 3.5, 3.6, and 3.7 some examples of the plots that can be obtained using the dimensionless and normalized quantities previously mentioned.

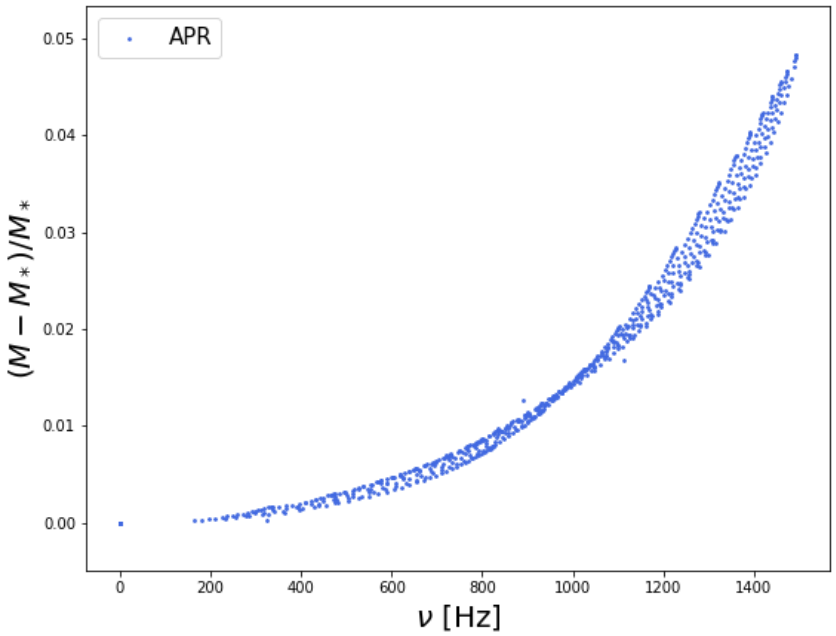

Figure 3.5: Sequences of fractional mass gained for rotating NSs with constant value of M_0. It is a function of the spin frequency. We considered the APR equation of state.

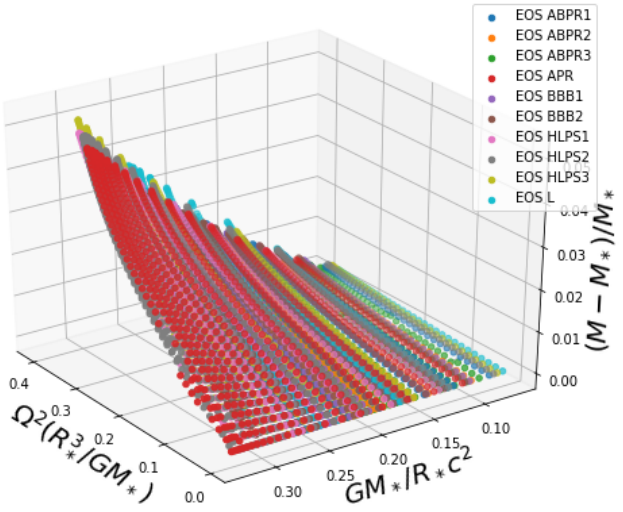

Figure 3.6: Fraction of total mass gained for ten EOS for rotating NSs, all of them as a function of the squared dimensionless angular velocity, and the dimensionless compactness.

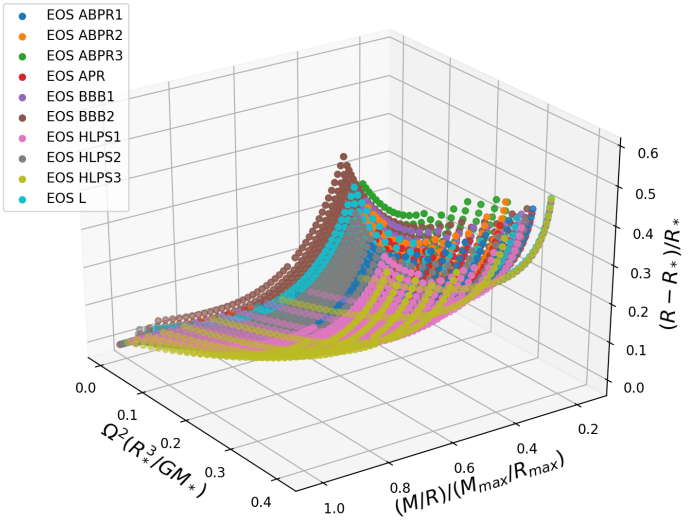

Figure 3.7: Fractional increase in radius as a function of the squared dimensionless angular velocity and normalized compactness. The ten EOS were considered.

Chapter 4

Fractional Increase in Mass

In general relativity, Einstein theorized that mass was not the only thing that curves spacetime, energy does as well. When a NS rotates it has a certain value of rotational kinetic energy, T. Thus it is logical to think that a NS gains a larger amount of mass as its spin frequency gets higher. In this chapter we are going to derive an approximation of this gain in mass, M, as a function of its intrinsic properties, like angular velocity, Ω, rest mass, M_0, and radius, R.

The various EOS can generally be divided into two types: *stiff* and *soft*. In simple terms, in a stiff EOS there is a large change in pressure for a given change in density, which means that NSs with stiff EOS are harder to compress and are more stable. On the other hand, soft EOS are easier to compress, and the change in pressure is not as big for the same given change in density. This means that NSs arising from soft EOS will not be as massive as NSs with stiff EOS, and that NSs with stiff EOS will have a larger radius than those with soft ones.

In Section 4.1 we are going to derive an order of magnitude approximation showing how the mass of a rotating NS changes compared to its value of rest mass, which is the mass of all the particles making up the NS. In Section 4.2 of this chapter we are going to derive an order of magnitude approximation for another increase in mass, but now compared to the mass of a static star with

the same rest mass. In Section 4.3 we numerically compute, using NSSS, these fractional increases in mass. We graphically analyse these relationship and we find a quasi-universal relation between said fractional increases in mass, and the angular velocity and compactness. In Section 4.4 we show the comparison of the changes in mass with the two recently discovered pulsars, MSP J0740+6620 and PSR J1614-2230.

4.1 Fractional Increase of Mass Compared to Rest Mass

We know that rotation modifies the shape of a NS and its X-ray emission (Morsink et al., 2007), but rotation also affects its mass, making it increase. This is because, as general relativity tells us, energy is also a source of gravity. A rotating NS has kinetic rotational energy, T, and combined with the gravitational binding energy, U, these energies modify the total mass of the star, M. Let us analyze how the mass of a NS changes when compared to its rest mass as it rotates. An approximation of this change in mass, considering relativistic sources is given by

$$M = M_0 + \frac{U}{c^2} + \frac{T}{c^2}. \tag{4.1}$$

We need the expressions for U and T. Let us assume that the NS is a sphere of uniform density, thus in this approximation, we take the Newtonian equation for U, then

$$U = -\frac{3}{5}\frac{GM_0^2}{R}, \tag{4.2}$$

$$T = \frac{1}{2}I\Omega^2, \tag{4.3}$$

where G is the gravitational constant, R is the equatorial radius, I is the moment of inertia of the NS, and Ω is the angular velocity.

Substituting (4.2) and (4.3) into (4.1) gives us the following relationship

$$M = M_0 - \frac{3}{5}\frac{GM_0^2}{Rc^2} + \frac{1}{2}\frac{I\Omega^2}{c^2}. \tag{4.4}$$

Replacing I for the moment of inertia of a solid sphere,

$$M = M_0 - \frac{3}{5}\frac{GM_0^2}{Rc^2} + \frac{1}{2}\left(\frac{2}{5}M_0R^2\right)\frac{\Omega^2}{c^2}, \tag{4.5}$$

$$= M_0\left(1 - \frac{3}{5}\frac{GM_0}{Rc^2} + \frac{1}{5}\frac{R^2\Omega^2}{c^2}\right). \tag{4.6}$$

Now, we multiply and divide the last term by R^3/GM_0,

$$M = M_0\left[1 - \frac{3}{5}\frac{GM_0}{Rc^2} + \frac{1}{5}\frac{R^2\Omega^2}{c^2}\left(\frac{R^3}{GM_0}\right)\left(\frac{GM_0}{R^3}\right)\right]. \tag{4.7}$$

Rewriting the last term on the right side,

$$M = M_0\left[1 - \frac{3}{5}\frac{GM_0}{Rc^2} + \frac{1}{5}\frac{R^2}{c^2}\left(\frac{\Omega^2R^3}{GM_0}\right)\left(\frac{GM_0}{R^3}\right)\right]. \tag{4.8}$$

We define now the following dimensionless angular velocity

$$\bar{\Omega}^2 = \frac{\Omega^2R^3}{GM_0}. \tag{4.9}$$

Thus, the mass of the NS becomes,

$$M = M_0\left[1 - \frac{3}{5}\frac{GM_0}{Rc^2} + \frac{1}{5}\frac{R^2}{c^2}\bar{\Omega}^2\left(\frac{GM_0}{R^3}\right)\right], \tag{4.10}$$

$$= M_0\left[1 - \frac{3}{5}\frac{GM_0}{Rc^2} + \frac{1}{5}\frac{GM_0}{Rc^2}\bar{\Omega}^2\right]. \tag{4.11}$$

Taking out the first term inside the brackets,

$$M = M_0 + M_0 \left[-\frac{3}{5}\frac{GM_0}{Rc^2} + \frac{1}{5}\frac{GM_0}{Rc^2}\bar{\Omega}^2 \right], \text{ leading to} \tag{4.12}$$

$$M - M_0 = M_0 \left[-\frac{3}{5}\frac{GM_0}{Rc^2} + \frac{1}{5}\frac{GM_0}{Rc^2}\bar{\Omega}^2 \right], \tag{4.13}$$

Therefore, the approximate fractional change in mass of a rotating NS due to relativistic sources compared to its rest mass is

$$\frac{M - M_0}{M_0} = \frac{GM_0}{Rc^2} \left[-\frac{3}{5} + \frac{1}{5}\bar{\Omega}^2 \right]. \tag{4.14}$$

This fractional change in mass has a negative slope, and it is directly proportional to the compactness of the NS. We can see that, as the spin frequency increases, the magnitude of this mass fraction will decrease.

4.2 Fractional Increase in Mass Compared to a Nonrotating NS

In the previous section we found that the approximate mass of a rotating NS depends on U and T. We will make use of the same approximation by taking into account the mass given by equation (4.4). Now we will analyse the change in mass from a different point of view, we will see how the total mass of a rotating NS changes compares to the total mass of a nonrotating NS, both with the same rest mass. The mass is then

$$M = M_0 - \frac{3}{5}\frac{GM_0^2}{Rc^2} + \frac{1}{5}\frac{M_0R^2}{c^2}\Omega^2. \tag{4.15}$$

Subtracting, on both sides, the mass of a nonrotating NS, M_*,

$$M - M_* = M_0 - M_* - \frac{3}{5}\frac{GM_0^2}{Rc^2} + \frac{1}{5}\frac{M_0R^2}{c^2}\Omega^2. \tag{4.16}$$

Multiplying and dividing the last term on the right side by R^3/GM_0,

$$M - M_* = M_0 - M_* - \frac{3}{5}\frac{GM_0^2}{Rc^2} + \frac{1}{5}\frac{M_0R^2}{c^2}\Omega^2\left(\frac{R^3}{GM_0}\right)\left(\frac{GM_0}{R^3}\right). \tag{4.17}$$

Dividing now by M_*,

$$\frac{M - M_*}{M_*} = \frac{M_0 - M_*}{M_*} + \frac{1}{M_*}\left[-\frac{3}{5}\frac{GM_0^2}{Rc^2} + \frac{1}{5}\frac{M_0R^2}{c^2}\left(\frac{GM_0}{R^3}\right)\bar{\Omega}^2\right]. \tag{4.18}$$

Rewriting the right side of the equation,

$$\frac{M - M_*}{M_*} = \frac{M_0 - M_*}{M_*} + \frac{1}{M_*}\left[-\frac{3}{5}\frac{GM_0^2}{Rc^2} + \frac{1}{5}\frac{GM_0^2}{Rc^2}\bar{\Omega}^2\right]. \tag{4.19}$$

We now know the fractional increase in mass of a rotating NS compared to the mass of a static NS,

$$\frac{M - M_*}{M_*} = \frac{M_0 - M_*}{M_*} + \frac{GM_0}{RC^2}\left[-\frac{3}{5}\frac{M_0}{M_*} + \frac{1}{5}\frac{M_0}{M_*}\bar{\Omega}^2\right]. \tag{4.20}$$

If we compare both fractional increases of mass as a NS rotates, we can see that (4.20) involves a fractional change in rest mass compared to the mass of a static NS. This means that this relation predicts a smaller change in mass than the one described by equation (4.14), in the previous section.

4.3 Graphical Analysis

After computing sequences of NSs with constant rest mass using NSSS, we can take a look at them and see how the mass of a NS increases as its angular velocity gets larger.

Figure 4.1 shows the fractional increase in total mass compared to the rest mass, this fractional change depends on the dimensionless angular velocity, $\Omega\left(R^3/GM\right)^{1/2}$. In this figure we have a set of sequences for EOS ABPR1 for different values of M_0. Each of the, approximately horizontal, rows of

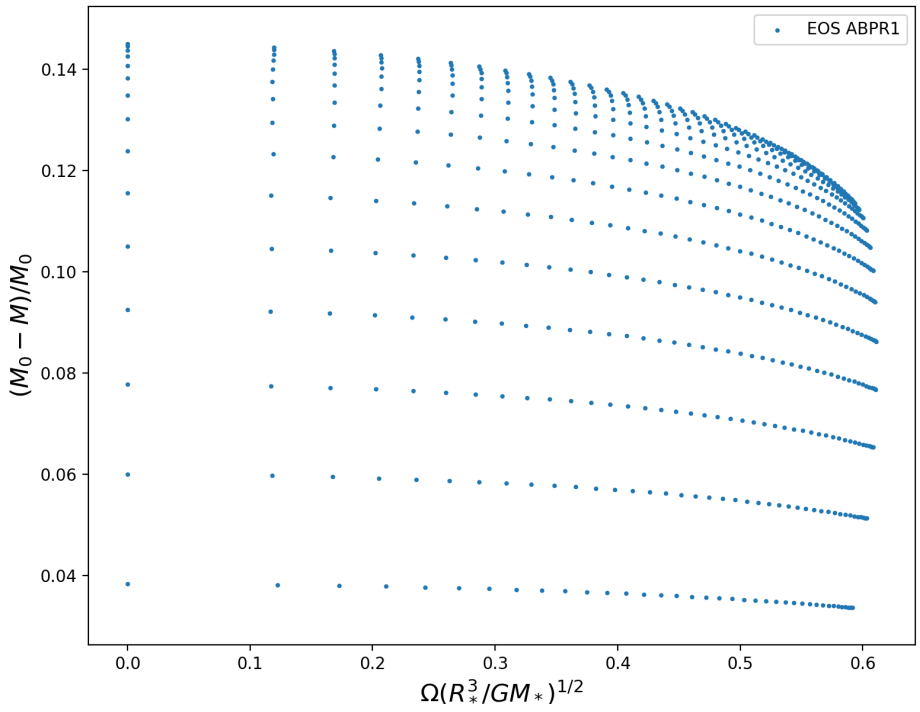

Figure 4.1: Fractional mass gain compared to the rest mass for ESO ABPR1. It is a function of the dimensionless angular velocity.

points corresponds to a constant rest-mass sequence of stars. The less massive sequences of NSs are located in the bottom of this plot, and the most massive on top.

A curious result is that, for the least massive sequence, the change in mass is almost non existent; this sequence is almost horizontal. Therefore we could even consider Newtonian mechanics to describe the less massive NSs. We can see that the lowest row of points is approximately linear with a negative slope, which is exactly the Newtonian approximation from equation (4.14). We see that relativistic effects are more dominant in high-mass sequences located at the top of the plot. Figure 4.2 shows all the sets of sequences for each of the ten EOS considered here. In this plot we can see that the maximum change in M with respect to M_0 is almost 20%.

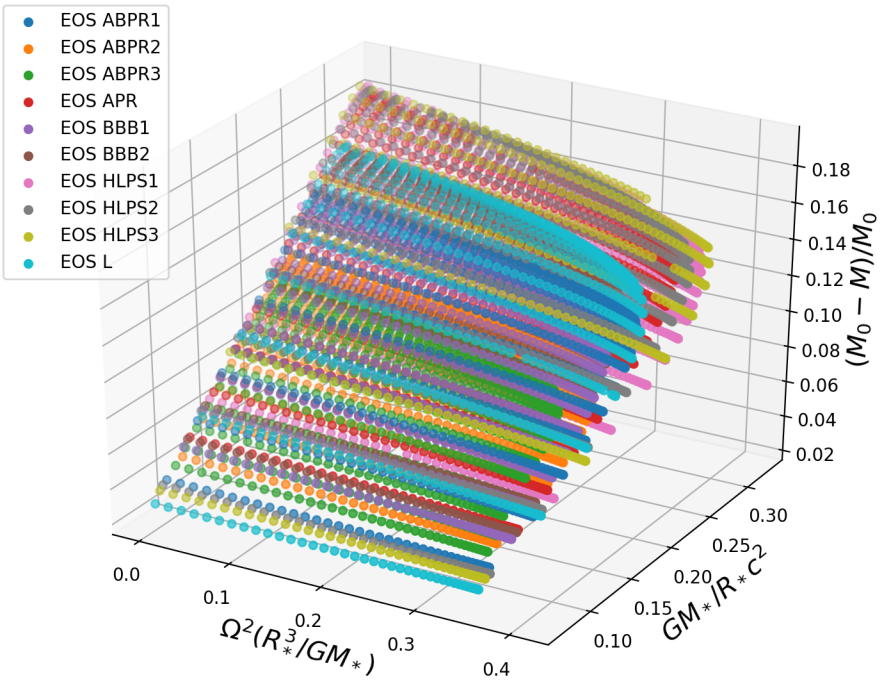

Figure 4.2: Fractional mass gain compared to the rest mass. It is a function of the squared dimensionless angular velocity and dimensionless compactness.

Figure 4.3 shows the change in mass of a NS compared to the mass of the nonrotating NS that begins each sequence. Each of them has the same value of M_0 for EOS ABPR1. We can see that the fractional change $(M - M_*)/M_*$ follows a squared increase compared to $(M - M_0)/M_0$, however the change is more significant in the latter. In the former, the fractional change in mass increases up to 3.5%.

The matter in a neutron star is degenerate, this means that the star is a very compact object, where the space between particles is close to the size of a neutron. This means that NSs with a high mass are smaller than those with a low mass. As a result, high-mass NSs have a higher increase in mass because they are more tightly bound together than lower-mass NSs, which results in a more gravitationally stable star. The considered EOS also plays a role here, if we have a stiff EOS, the star can be held together easily as it rotates, which results in a higher increase in mass before it breaks apart.

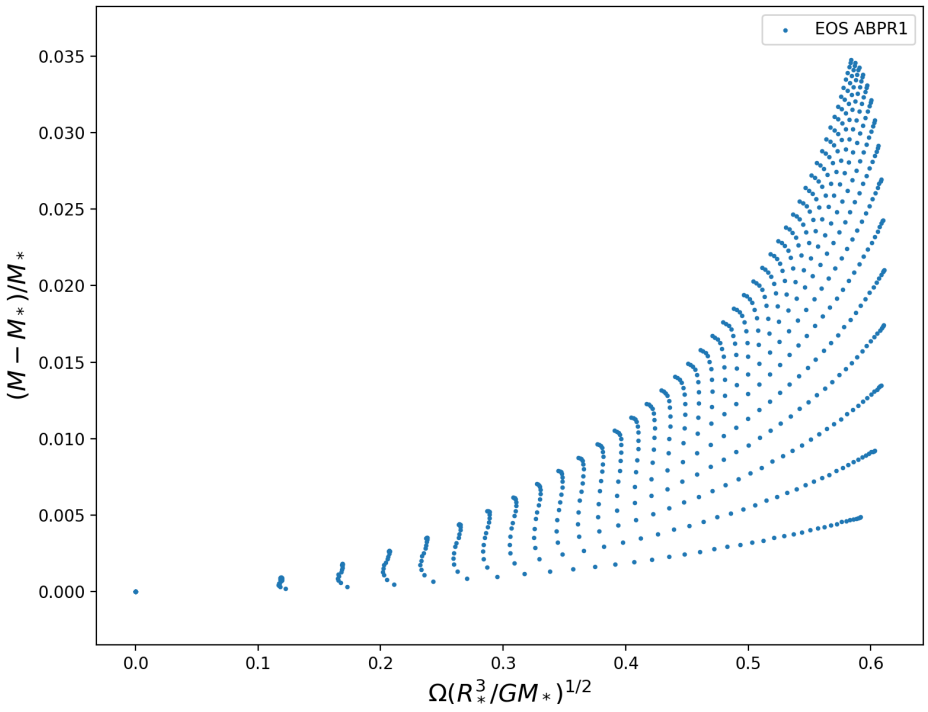

Figure 4.3: Fractional mass gain compared to the mass of a nonrotating NS for EOS ABPR1. It is a function of the dimensionless angular velocity.

In Figure 4.4 we can see the same fractional increase in mass as in Figure 4.3, but this time as a function of the dimensionless squared angular velocity and the dimensionless compactness. It shows a clear trend, where the maximum increase in mass is approximately 5% for all EOS.

If we focus our attention on the 3D plots in Figures 4.2 and 4.4 we see that either fractional change in mass follows a clear trend. Thus it is possible to find a surface that best fits all the sequences for all the EOS. The equation of the surface (shown in Figure 4.5 and 4.6 for two different angles of visualization)

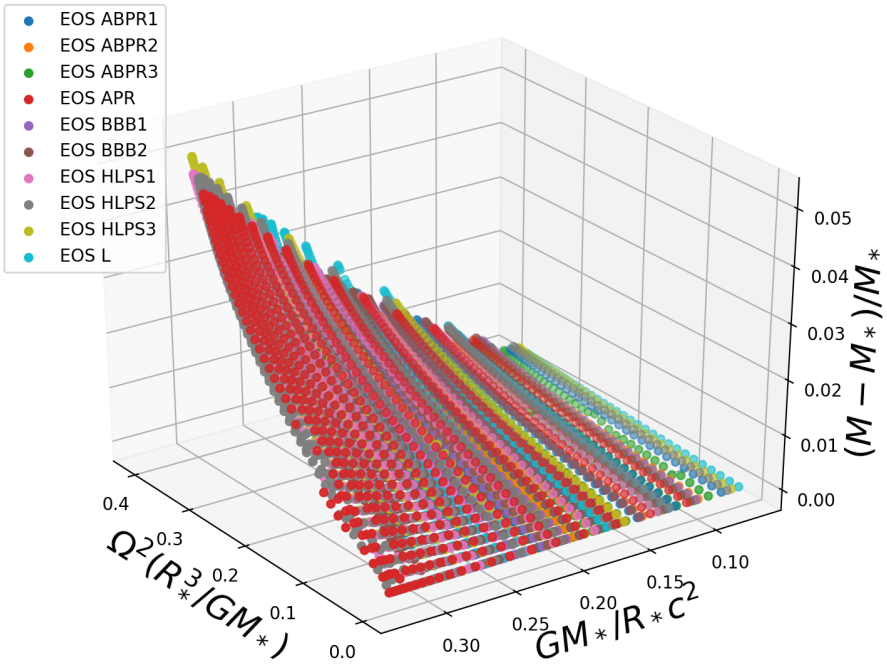

Figure 4.4: Fractional mass gain compared to the mass of a nonrotating NS, considering ten EOS. It is a function of the squared dimensionless angular velocity and dimensionless compactness.

that best approximates the data of $(M - M_0)/M_0$ is given by

$$\begin{aligned}\frac{M_0 - M}{M_0} = &-0.015 + 0.893y - 3.725y^2 + 15.991y^3 - 22.045y^4 + \\ &x\left[-0.211 + 1.386y - 3.947y^2 + 3.314y^3\right] + \\ &x^2\left[1.709 - 6.443y + 3.943y^2\right] + \\ &x^3\left[-5.459 + 9.348y\right] + 5.906x^4,\end{aligned} \tag{4.21}$$

where

$$x = \Omega^2\left(\frac{R_*^2}{GM_*}\right), \tag{4.22}$$

$$y = \frac{GM_*}{Rc^2}. \tag{4.23}$$

We chose an even power for the polynomial fitting because the change in

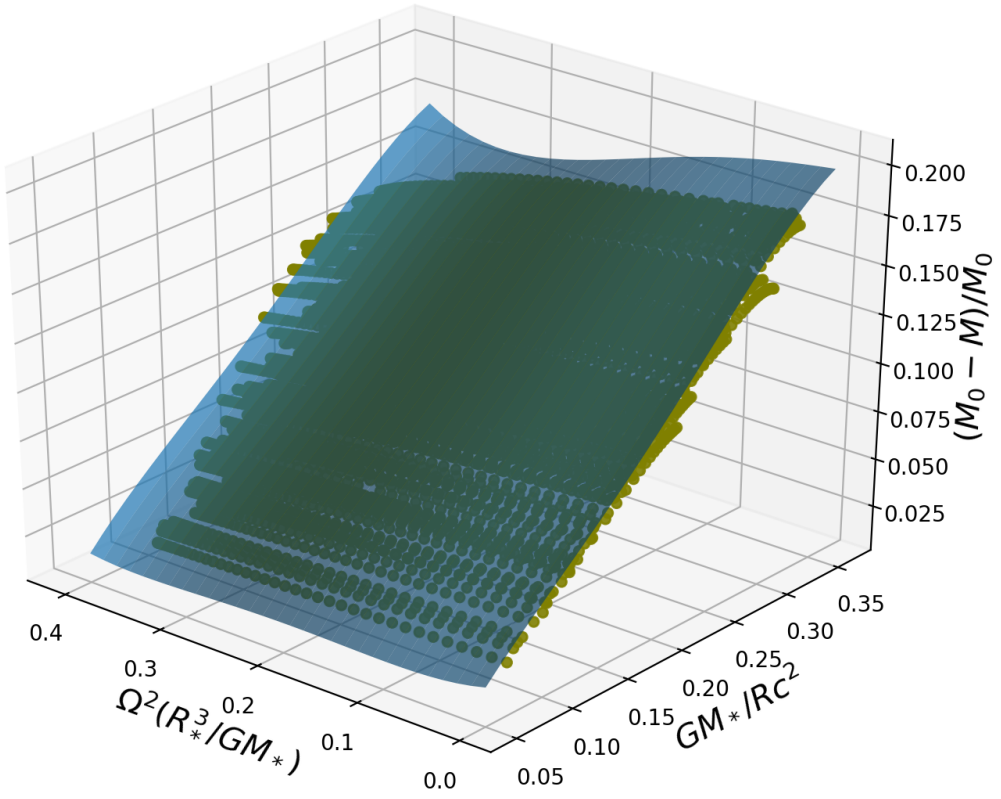

Figure 4.5: Best fit surface of the data for $(M_0 - M)/M_0$ for the ten EOS considered in this work.

mass described by equation 4.14 depends on the squared angular velocity. To estimate how good the fit is, we use the coefficient of determination[1], R^2, which is the proportion of the variance in the dependent variable ($(M - M_0)/M_0$, in this case) that is predictable from the independent variable (angular velocity and compactness). It follows the condition $0 \leq R^2 \leq 1$, with $R^2 = 1$ being the surface that matches exactly the behaviour of the data, and $R^2 = 0$ represents the surface that does not fit the data at all. For this fit, the coefficient of determination is $R^2 = 0.95719$, which means that is close to being an perfect fit.

Now, the surface that best approximates the behaviour of the second frac-

[1]Python documentation for R^2. `https://scikit-learn.org/stable/modules/model_evaluation.html#r2-score`

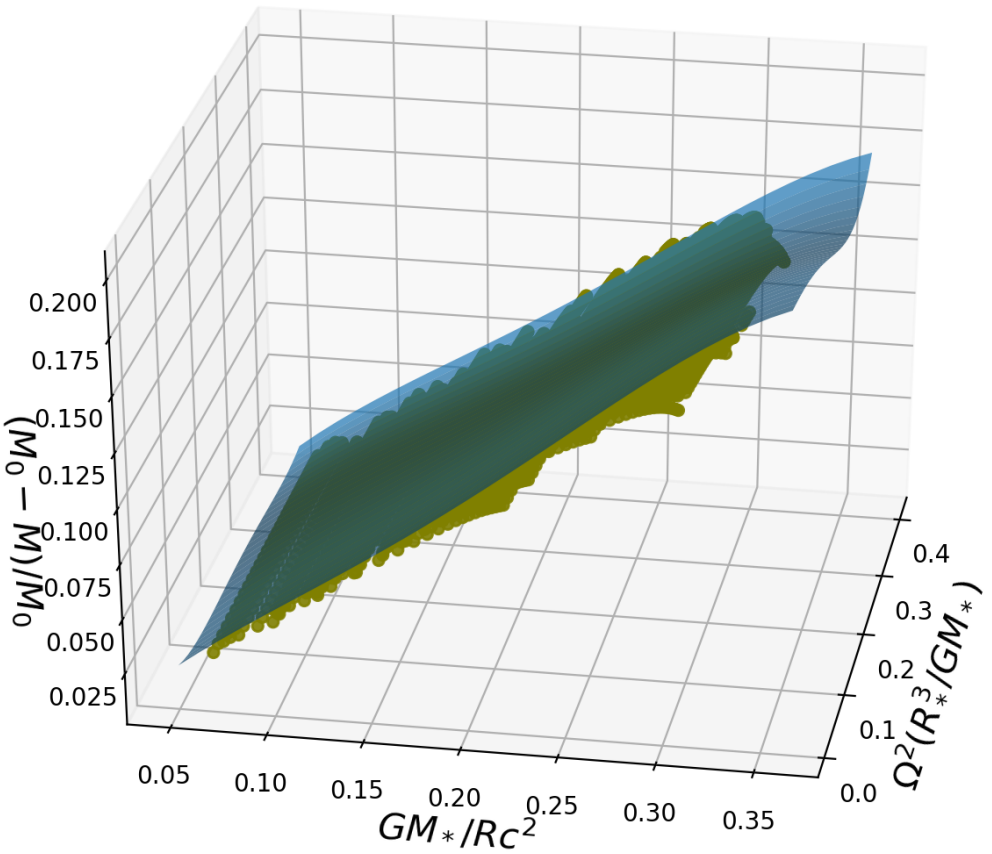

Figure 4.6: A different view of the best fit surface of the data for $(M_0 - M)/M_0$ for the ten EOS considered in this work.

tional change, $(M - M_*)/M_*$ (Figures 4.7 and 4.8 show two different angles of visualization), is given by

$$\begin{aligned}\frac{M - M_*}{M_*} = &-0.004 + 0.034y - 0.152y^2 + 0.491y^3 - 0.729y^4 + \\ &x\left[0.109 - 0.274y + -0.255y^2 + 2.693y^3\right] + \\ &x^2\left[-0.966 + 2.739y + 0.089y^2\right] + \\ &x^3\left[2.903 - 3.596y\right] - 2.978x^4, \end{aligned} \tag{4.24}$$

where x and y are the same as the previously defined variables. For this best fit surface equation we get a coefficient of determination of $R^2 = 0.97869$, which is in a better agreement with the data than the previous surface equation, (4.21).

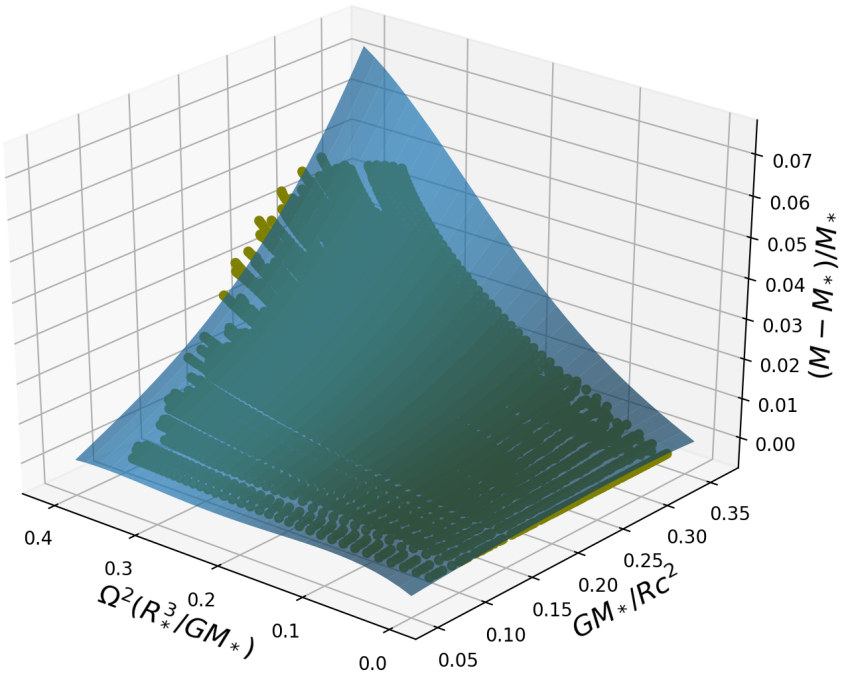

Figure 4.7: Best fit surface of the data for $(M - M_*)/M_*$ for the ten EOS considered in this work.

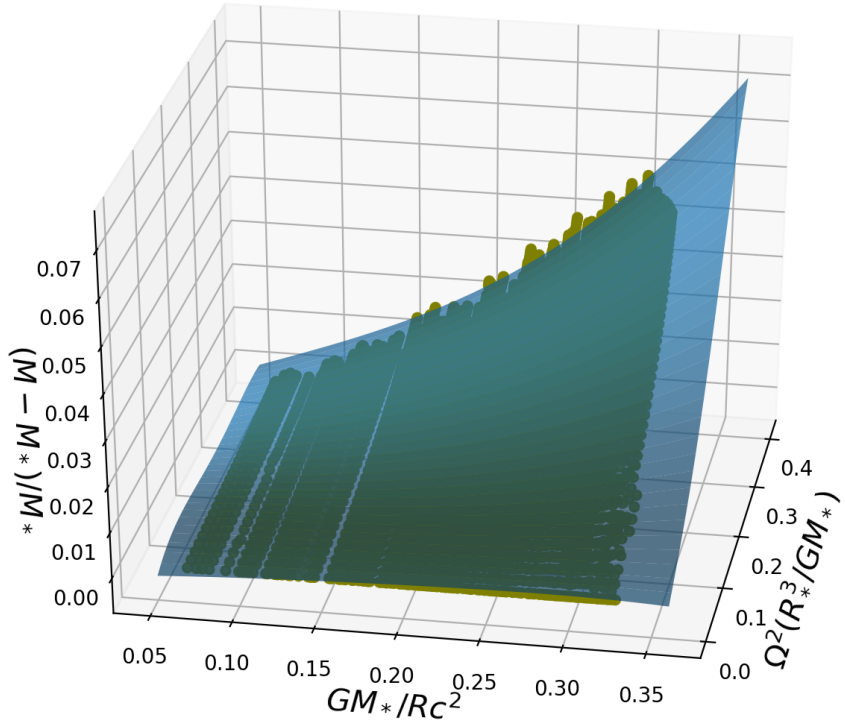

Figure 4.8: Another view of the best fit surface of the data for $(M - M_*)/M_*$ for the ten EOS considered in this work.

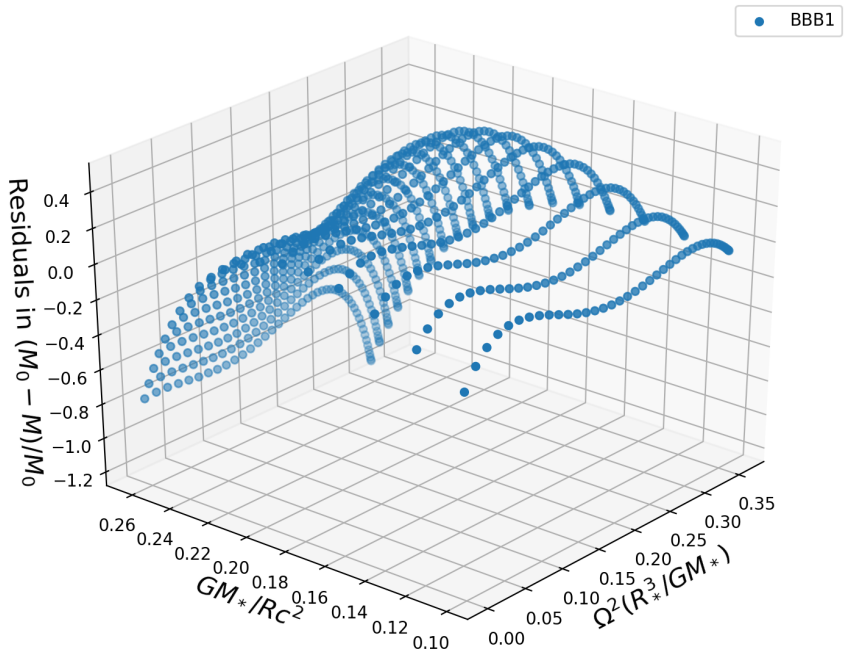

Figure 4.9: Residual percentages for EOS BBB1 and the $(M - M_0)/M_0$ surface, described by equation (4.21).

To check whether the equations for best fit surface, (4.21) and (4.24), are a good fit, we compute the residuals between these equations and the data from each EOS. In Figure 4.9 we have the residuals for $(M - M_0)/M_0$ for EOS BBB1, and in Figure 4.10 we see the residuals for $(M - M_*)/M_*$ considering EOS APR. We consider those two EOS because they are the ones that have the least amount of difference between the surface and the data. The residuals for $(M-M_0)/M_0$ vary from 0.4% to 2.5%, while the residuals for $(M-M_*)/M_*$ vary from 0.1% to 1%, which means that, in all the EOS, both fractional changes in mass are independent of the EOS.

The trend that both fractional changes follows makes us think that it has something to do with universality. Universal relations have being found between the deviations of the effective acceleration due to gravity, the compactness, the dimensionless squared angular velocity and the latitude on the star's surface (Yagi & Yunes, 2013); or a universal relation between the moment of inertia, the Love number and the quadrupole moment, which are independent

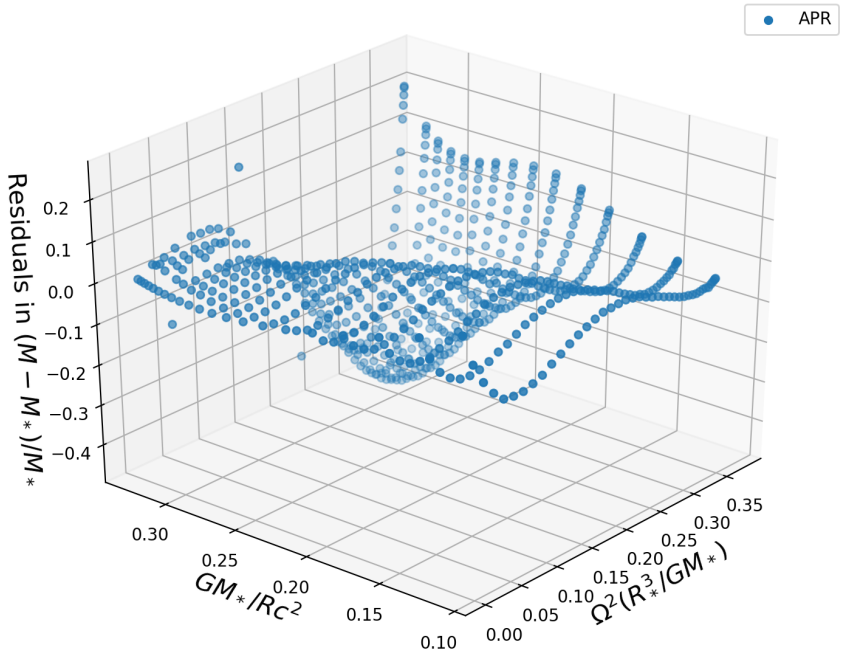

Figure 4.10: Residual percentages for EOS APR and the $(M - M_*)/M_*$ surface, described by equation (4.24)

of the neutron star's internal structure (AlGendy & Morsink, 2014).

This time we found a universal relations for $(M - M_0)/M_0$ and $(M - M_*)/M_*$, both dependent on the dimensionless squared angular velocity, $\Omega^2 R^3/GM$, and the dimensionless compactness, GM/Rc^2. Both of these relations are nearly independent of the EOS used.

We are assuming that NSs are uniformly rotating, which means that we consider them to be rigid bodies, where each part of it is rotating at the same speed. On the other hand, differential rotation in NSs means that different parts of a NS will rotate at different rates, like the Sun, where areas on the surface in the poles rotate at a faster rate than areas in the equator. Differential rotation is not very likely to happen in NSs, although the merger of two NSs could result in a differentially rotating super massive neutron star (Morrison et al., 2004), where the fractional changes in mass could reach up to a 50% increase respect to the rest mass (Kaplan et al., 2014), while the increase in uniformly rotating NSs, as we have seen before, reaches 20%.

Another consequence of differential rotation are glitches, which are a sudden change in the rotation of a NS. These have been observed to happen in the Vela pulsar in 2016 and in the Crab pulsar in 2017 (Keitel et al., 2019), which leads to the conclusion that there is a superfluid in the interior of these massive objects, that rotates at a different rate below the solid crust, and when the two catch up, a glitch is observed.

4.4 Comparison with High Mass Pulsars

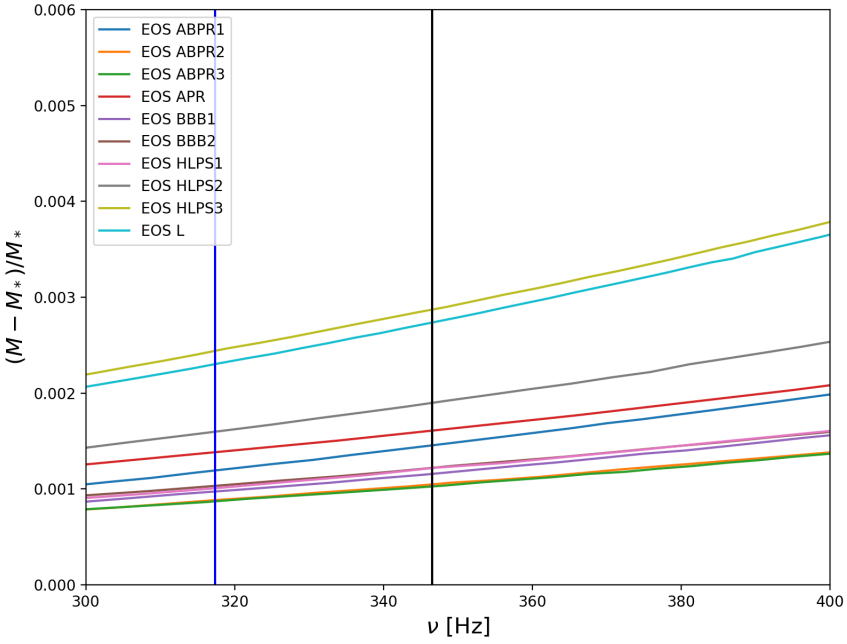

Figure 4.11: Mass fraction of all equations of estate showing the pulsars MSP J0740+6620 (black vertical line), and PSR J1614-2230 (blue vertical line).

We can use some of the sequences to compare with two recently discovered pulsars, MSP J0740+6620 (Cromartie et al., 2019a) with a total mass of $M = 2.17^{+0.11}_{-0.10}$ $M_\odot$ and $\nu = 346.5319$ Hz; and PSR J1614-2230 (Demorest et al., 2010), with a mass of $M = 2.01 \pm 0.04$ $M_\odot$ and a rotational frequency of $\nu = 317.379$ Hz. Both of them are millisecond pulsars (MSP), which are a type

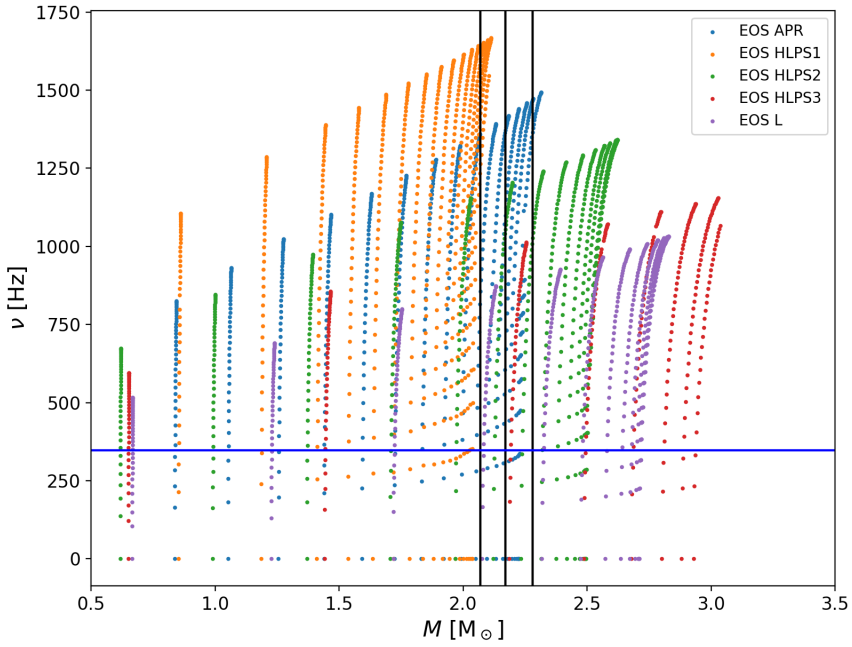

Figure 4.12: Frequency as a function of mass of the neutron stars computed here. The black vertical lines represent the 1σ range in the mass of MPS J0740+6620; the black central vertical line is the central value, $M = 2.17\ \mathrm{M}_\odot$. The blue horizontal line represents its spin frequency, $\nu = 346.5319$.

of neutron stars that have a period in a range of 1-10 milliseconds. Since we cannot measure M_0, we compare the sequences of $(M - M_*)/M_*$ with these two discoveries. In Figure 4.11 we can see the ten maximum-mass sequences and the location of both pulsars' spin frequency, the black vertical line is MSP J0740+6620, and the blue vertical line represents PSR J1614-2230. We can notice that the stiffest EOS (HLPS3 and L) are above the rest that follow a similar rate of change. The changes in mass for both of the millisecond pulsars are less than 0.3%.

Similarly, in Figure 4.12 we can see a plot of ν as a function of the mass of the NSs (the sequences of stars are now vertical). In this, we plot the data for MSP J0740+6620 as a comparison. The black vertical lines represent $(2.07\,\mathrm{M}_\odot,\ 2.28\,\mathrm{M}_\odot)$, or in other words, the 1σ measurement in the mass of

the pulsar. The majority of the EOS in the plot are stiff which, as we know, allow a NS to have a larger mass, in this case more than $2\,M_{\odot}$. Those five EOS shown (APR, HLPS1, HLPS2, HLPS3, L) are the only ones in our library that reach a maximum mass above $2\,M_{\odot}$. We can also see that EOS HLPS1 is almost ruled out by the 1σ mass limit. However, more observations of this pulsar are required to reduce the size of the error bars on the mass. For the relatively low spin rate of 346.53 Hz, the change in mass caused by rotation is insignificant. This means that the upper mass limit derived from the TOV equations is sufficient to use this pulsar's mass to rule out any EOS.

Chapter 5

Fractional Increase in Radius

Similarly to the previous chapter, we will analyse a fractional increase, but now it will be in the equatorial radius of a NS as it spins, $(R - R_*)/R_*$. With this ratio we investigate how the equatorial radius, R, increases compared to the radius of a nonrotating NS, R_*. Both of the radii involved in the fractional change belong to a sequence of NSs with the same value of M_0.

In Figure 5.1 we can see the fractional change in radius as a function of the dimensionless angular velocity. In this plot, the sequences are shown as continuous lines instead of individual points that represent the stars, this is done to see, in a better way, the behaviour of the sequences. We can notice that all of them approach an asymptote, this is the Kepler limit. Close to this limit is where the largest rate of growth in radius occur, and as we can see, it can get to 40% larger than a nonrotating NS, in the case of EOS APR.

The three-dimensional plot in Figure 5.2 is the graph of all the sequences with constant M_0, considering the ten EOS. In this plot we can see the fractional increase in radius as a function of dimensional variables, the squared value of the angular velocity and the compactness, GM_*/R_*c^2.

Looking at Figure 5.2 we see that the rates of change define a surface, because there is a clear trend in all the sequences. Thus we do a similar analysis to that of Chapter 4, and we find that the best fit surface to these points does

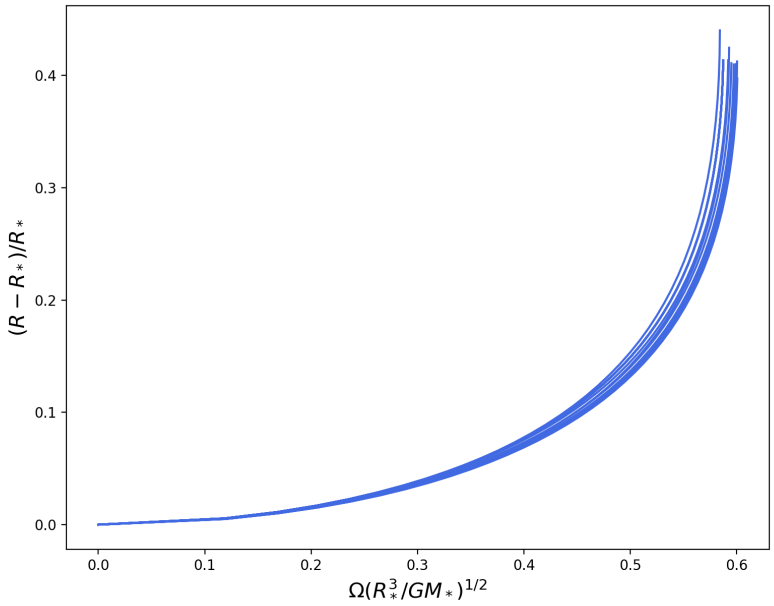

Figure 5.1: Fractional increase in radius as a function of the dimensionless angular velocity. The sequences are represented as lines for EOS APR.

not represent a good fit compared the previous fractional changes in mass in chapter 4, where we obtained values of R^2 close to one (which means perfect fit). Due to this issue we make another plot to do the same analysis. This new plot is found in Figure 5.3, where $(R-R_*)/R_*$ is now a function of the dimensionless squared angular velocity, and the normalized compactness, $(M/R)/(M_M/R_M)$, where M_M, and R_M are the mass and radius of the maximum-mass NS for each EOS.

Taking into account the new fractional change in Figure 5.3, we construct a best fit surface that can be seen in Figure 5.4. This surface is described by

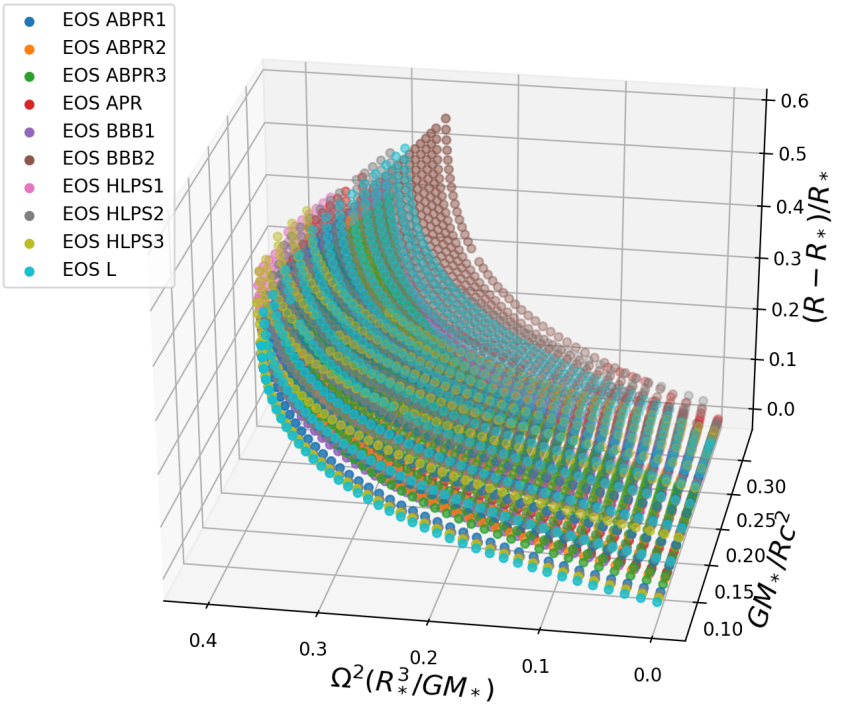

Figure 5.2: Fractional increase in radius as a function of the squared dimensionless angular velocity and dimensionless compactness. The ten EOS were considered.

the following equation

$$\begin{aligned}\frac{R-R_*}{R_*} = &-1.079 + 7.230y - 16.945y^2 + 16.525y^3 - 5.723y^4 + \\ &x\left[10.218 - 39.826y + 57.450y^2 - 27.006y^3\right] + \\ &x^2\left[-44.715 + 73.352y - 40.445y^2\right] + \\ &x^3\left[121.997 - 63.912y\right] - 118.469x^4, \end{aligned} \tag{5.1}$$

where x and y are given by

$$x = \Omega^2\left(\frac{R_*^2}{GM_*}\right), \tag{5.2}$$

$$y = \frac{M/R}{M_M/R_M}. \tag{5.3}$$

This equation of the best fit surface has a coefficient of determination of

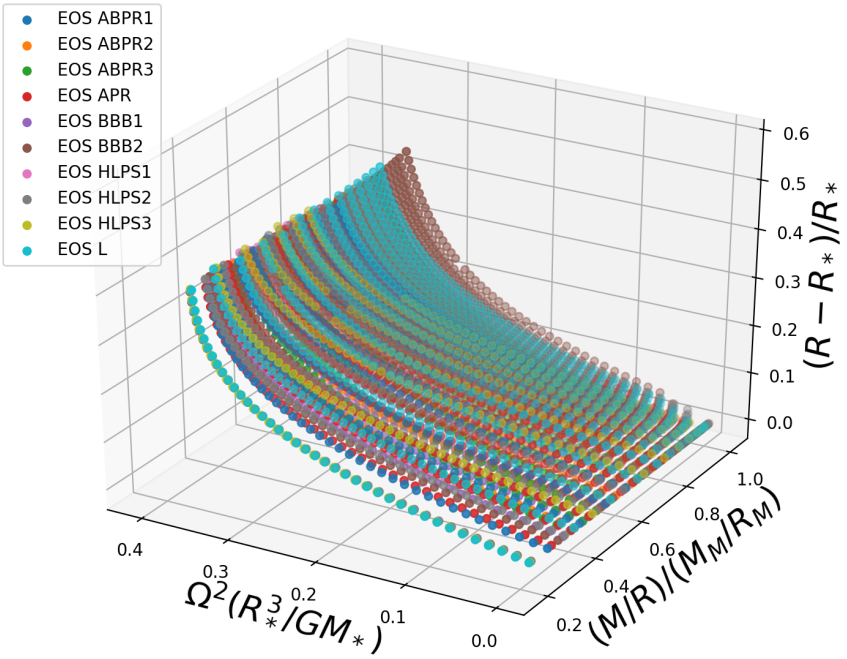

Figure 5.3: Fractional increase in radius as a function of the squared dimensionless angular velocity and normalized compactness. The ten EOS were considered.

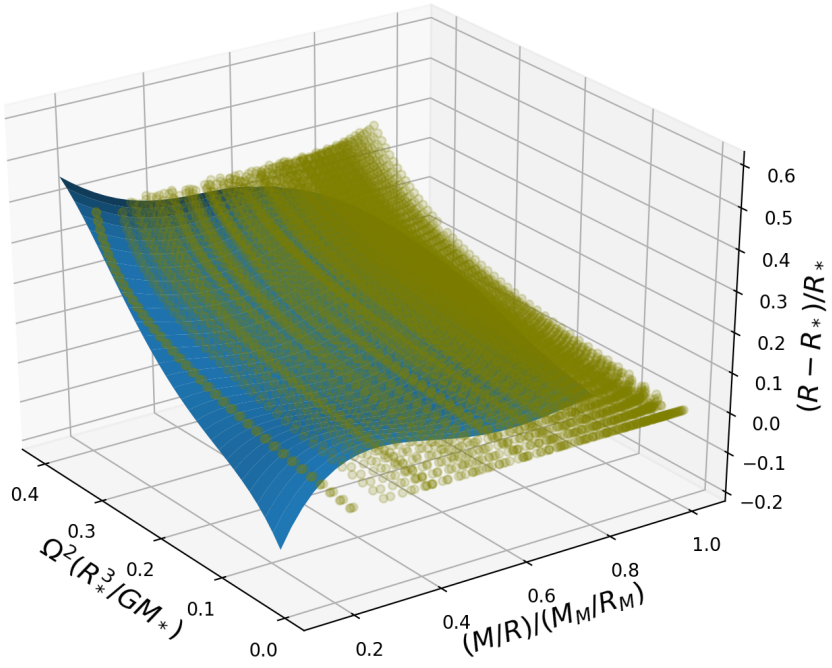

Figure 5.4: Best fit surface of the data for $(R - R_*)/R_*$ for all equations of state considered in this work.

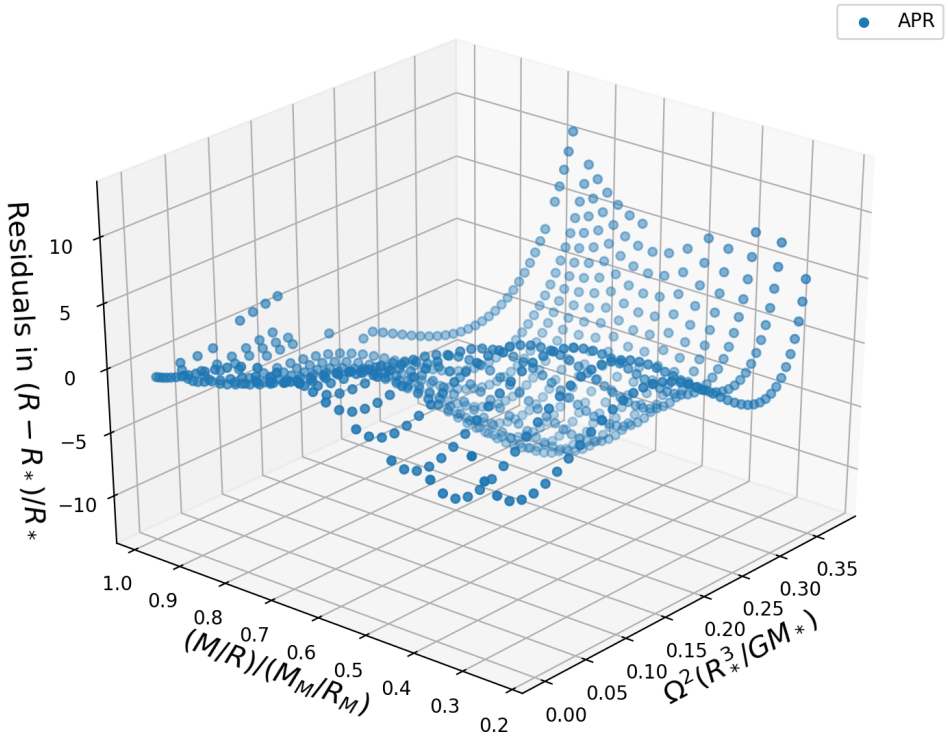

Figure 5.5: Residual percentages for EOS APR and the $(R - R_*)/R_*$ surface, described by equation 5.1.

$R^2 = 0.77769$. This value is close to the one corresponding to the NS sequences in Figure 5.2, which is $R^2 = 0.76808$.

The best fit surface follows, in a good way, the behaviour of the data points, so let us compute the residuals (Figure 5.5) between the surface equation (5.1) and the data from EOS APR.

Unlike the residuals for mass in Chapter 4, the residuals for radii are not small, they vary from 10% to 40%. This means that all the sequences follow a trend, specially in the regions were $\Omega^2(R_*^3/GM_*) \lesssim 0.2$, which shows that $(R - R_*)/R_*$ is almost independent of the EOS considered. The trend suggests a possible universality, similar to previous studies done by AlGendy & Morsink (2014), and Yagi & Yunes (2013)). Equation (5.1) describes only a quasi-universal relation, one that is only dependent of dimensionless variables, the squared angular velocity, $\Omega^2 R^3/GM$, and the normalized compact-

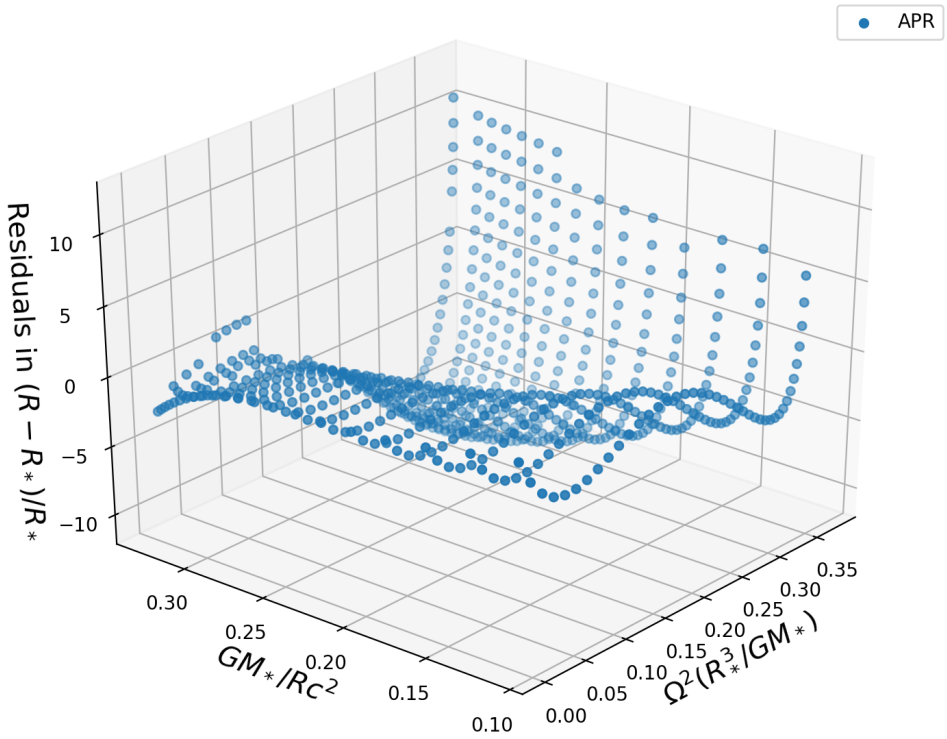

Figure 5.6: Residual percentages for EOS APR and the $(R - R_*)/R_*$ surface considering the data from Figure 5.2. It is a function of $\Omega^2 R^3/GM$ and GM_*/Rc^2.

ness, $(M/R)/(M_M/R_M)$.

Both fractional increases in radius considered here (one as a function of GM_*/R_*c^2, and the other as a function of $(M/R)/(M_M/R_M)$) vary significantly compared to the fractional change in mass. Let us consider the data that depends on GM_*/R_*c^2 and the dimensionless squared angular velocity. We can see in Figure 5.6 the residuals for EOS APR, which are the smallest (up to 10%) among the ten EOS. The majority of them have residuals that go up to 40%. A way to find a better fit would be to only use data that goes up to $\Omega^2(R_*^3/GM_*) \lesssim 0.2$, which represents, approximately, $\nu = 800$ Hz. This would be a better fit because the rapid increase in R occurs at higher values of spin frequency, and nowadays, there have been no observations of NSs that rotate faster than $\nu = 800$ Hz. The fastest spinning pulsar has a spin frequency of $\nu = 716$ (Hessels et al., 2006).

Chapter 6

Conclusions

We know the relation between mass and radius of neutron stars for a given EOS when the star is static. For every single one of them there is a different value of mass and radius. But things change when the NS rotates, relativistic effects will change the relationship between mass and radius. That is why it it important to understand the effects rotation has on a NS's mass and radius.

There was a small difference between both of the fractional changes in mass, $(M - M_0)/M_0$ and $(M - M_*)/M_*$. In the first one we obtained residuals up to 2.5% when compared to the best fit surface. In the second case we got residuals of less than 1%. This difference is due to the intrinsic difference in total mass and rest mass. The latter is around 15% larger than the former. On the other hand, compared to a non rotating star, the radius of a rotating NS increases to below 50% before reaching the Kepler limit and breaking apart.

We found that both fractional changes, in mass and radius, follow a trend, no matter which EOS we are working with. This is telling us that there is a universal relationship in the changes in mass and radius, which depend on the dimensionless value of the squared angular velocity, and either the dimensionless compactness, or the normalized NS's compactness. These relationships are clearly more accurate for the fractional changes in mass than for those in radius.

In the case of the fractional increase in radius, we notice that the surface is in good agreement with the data that meets the condition $\Omega^2(R_*^3/GM_*) \lesssim 0.2$. This is because, for spin frequencies higher than $\nu \approx 800$ Hz, the change in R increases almost exponentially, and as of today, there had not been observations of NSs with spin frequencies higher than that.

The future of NS observation is looking promising, new telescopes and projects (NICER, eXTP, STROBE-X) are being developed to obtain more accurate observations of NSs. The simulations in this work will help us compare the results obtained here with the observations, which will be helpful to constrain the number of EOS to a more appropriate equation to describe a NS's interior.

Appendix A

Equations of Stellar Structure for Rotating Neutron Stars

The metric considered to compute rotating neutron stars with axial symmetry is Cook et al. (1992)

$$ds^2 = -e^{\gamma+\rho}dt^2 + e^{2\alpha}\left(dr^2 + r^2 d\theta^2\right) + e^{\gamma-\rho}r^2\sin^2\theta(d\phi - \omega dt)^2, \qquad \text{(A.1)}$$

where the potentials ρ, γ, α and ω are functions of r and θ. Notice that we are following the notation from Komatsu et al. (1989). To compute NSs it is considered that $G = c = 1$. The matter is assumed to be a perfect fluid with a stress-energy tensor given by the following

$$T^{\mu\nu} = (\rho_0 + \rho_i + P)\, u^\mu u^\nu + P g^{\mu\nu}, \qquad \text{(A.2)}$$

where ρ_0 is the rest-energy density, ρ_i is the internal energy density, P is the pressure, and u^μ is the four-velocity. The Einstein Field equations to solve for

the potentials ρ, γ and ω are

$$\nabla^2 \left[\rho e^{\gamma/2}\right] = S_\rho(r,\mu), \tag{A.3}$$

$$\left(\nabla^2 + \frac{1}{r}\partial_r - \frac{\mu}{r^2}\partial_\mu\right)\left[\gamma e^{\gamma/2}\right] = S_\gamma(r,\mu) \quad \text{and} \tag{A.4}$$

$$\left(\nabla^2 + \frac{2}{r}\partial_r - \frac{2\mu}{r^2}\partial_\mu\right)\left[\omega e^{(\gamma-2\rho)/2}\right] = S_\omega(r,\mu), \tag{A.5}$$

where ∇^2 is the Laplacian in a flat space with spherical coordinates, $\mu = \cos\theta$, and S_ρ, S_γ, and S_ω are source functions, which can be found in Komatsu et al. (1989), along with the definition of the metric potential α.

To find the metric potentials the code first starts by having initial guesses for all of them, which come from the spherical solutions of the TOV equations. Then it tries different values of the equatorial radius to find the suitable shape of the star. Then, the code computes new values of the potentials in a following iteration. The solution if found when the difference of each quantity between two successive cycles becomes sufficiently small.

Bibliography

Abbott, B. P., Abbott, R., Abbott, T. D., et al. 2017, PRL, 119, 161101

Akmal, A., Pandharipande, V. R., & Ravenhall, D. G. 1998, Physical Review C, 58, 1804

Alford, M., Braby, M., Paris, M., & Reddy, S. 2005, ApJ, 629, 969

AlGendy, M., & Morsink, S. M. 2014, ApJ, 791, 78

Amason, C. 2019, Master's thesis, University of Alberta, 116 St & 85 Ave, Edmonton, AB T6G 2R3, master thesis

Baade, W., & Zwicky, F. 1934, Proceedings of the National Academy of Science, 20, 259

Baldo, M., Burgio, G. F., & Bombaci, I. 1996, arXiv e-prints, nucl

Bally, J., & Reipurth, B. 2006, The Birth of Stars and Planets (Cambridge University Press), 206,207. https://books.google.ca/books?id=Pwy9OtT8u6QC

Chakrabarty, D. 2008, in American Institute of Physics Conference Series, Vol. 1068, American Institute of Physics Conference Series, ed. R. Wijnands, D. Altamirano, P. Soleri, N. Degenaar, N. Rea, P. Casella, A. Patruno, & M. Linares, 67–74

Comella, J. M., Craft, H. D., Lovelace, R. V. E., & Sutton, J. M. 1969, NAT, 221, 453

Condon, J., & Ransom, S. 2016, Essential Radio Astronomy, Princeton Series in Modern Observational Astronomy (Princeton University Press), 214,215. https://books.google.ca/books?id=Jg6hCwAAQBAJ

Cook, G. B., Shapiro, S. L., & Teukolsky, S. A. 1992, ApJ, 398, 203

—. 1994, ApJ, 424, 823

Cromartie, H. T., Fonseca, E., Ransom, S. M., et al. 2019a, arXiv e-prints, arXiv:1904.06759

Cromartie, H. T., Fonseca, E., Ransom, S. M., et al. 2019b, Nature Astronomy, 1. https://www.nature.com/articles/s41550-019-0880-2

Danilenko, A. A., Zyuzin, D. A., Shibanov, Y. A., & Zharikov, S. V. 2011, MNRAS, 415, 867

Demorest, P. B., Pennucci, T., Ransom, S. M., Roberts, M. S. E., & Hessels, J. W. T. 2010, Nature, 467, 1081

Haardt, F., Gorini, V., Moschella, U., Treves, A., & Colpi, M. 2015, Astrophysical Black Holes, Lecture Notes in Physics (Springer International Publishing), 4. https://books.google.ca/books?id=ALjfCgAAQBAJ

Haensel, P., Potekhin, A., & Yakovlev, D. 2007, Neutron Stars 1: Equation of State and Structure, Astrophysics and Space Science Library (Springer New York), 25,41. https://books.google.ca/books?id=fgj_TZ06niYC

Hartle, J. B. 1978, Physics Reports, 46, 201

Hebeler, K., Lattimer, J. M., Pethick, C. J., & Schwenk, A. 2013, ApJ, 773, 11

Heinke, C. O., Cohn, H. N., Lugger, P. M., et al. 2014, Monthly Notices of the Royal Astronomical Society, 444, 443. https://doi.org/10.1093/mnras/stu1449

Hessels, J. W. T., Ransom, S. M., Stairs, I. H., et al. 2006, Science, 311, 1901

Hewish, A., Bell, S. J., Pilkington, J. D. H., Scott, P. F., & Collins, R. A. 1968, NAT, 217, 709

Kaaret, P., Prieskorn, Z., in 't Zand, J. J. M., et al. 2007, ApJ, 657, L97

Kaplan, J. D., Ott, C. D., O'Connor, E. P., et al. 2014, ApJ, 790, 19

Keitel, D., Woan, G., Pitkin, M., et al. 2019, arXiv e-prints, arXiv:1907.04717

Komatsu, H., Eriguchi, Y., & Hachisu, I. 1989, Monthly Notices of the Royal Astronomical Society, 237, 355

Kraus, U. 1998, in Relativistic Astrophysics, 66–81

Lattimer, J. M., & Prakash, M. 2001, ApJ, 550, 426

Lattimer, J. M., & Prakash, M. 2004, Science, 304, 536. https://science.sciencemag.org/content/304/5670/536

Linares, M., Shahbaz, T., & Casares, J. 2018, ApJ, 859, 54

Longair, M. 2011, High Energy Astrophysics (Cambridge University Press), 401–406. https://books.google.ca/books?id=KGe3FVbDNk4C

Lorimer, D. R., & Becker, W. 2009, Neutron Stars and Pulsars, 1st edn., Astrophysics and space science library 357 (Springer-Verlag Berlin Heidelberg), 95. http://gen.lib.rus.ec/book/index.php?md5=1272810CA36525E47BFA03D065FAABC5

Lorimer, D. R., & Kramer, M. 2004, Handbook of Pulsar Astronomy, Vol. 4, 28

Margalit, B., & Metzger, B. D. 2017, ApJ, 850, L19

Morrison, I. A., Baumgarte, T. W., & Shapiro, S. L. 2004, ApJ, 610, 941

Morsink, S. M., Leahy, D. A., Cadeau, C., & Braga, J. 2007, ApJ, 663, 1244

Nollert, H. P., Ruder, H., Herold, H., & Kraus, U. 1989, AAP, 208, 153

Oppenheimer, J. R., & Volkoff, G. M. 1939, Phys. Rev., 55, 374. https://link.aps.org/doi/10.1103/PhysRev.55.374

Özel, F., & Freire, P. 2016, Annual Review of Astronomy and Astrophysics, 54, 401

Ozel, F., & Psaltis, D. 2009, Physical review D: Particles and fields, 80, doi:10.1103/PhysRevD.80.103003

Özel, F., Psaltis, D., Ransom, S., Demorest, P., & Alford, M. 2010, ApJL, 724, L199

Page, D. P., Prakash, M., Lattimer, J., & Steiner, A. 2011, in Brazilian Workshop on Nuclear Physics (XXXIV BWNP), 5

Pandharipande, V. R., Pines, D., & Smith, R. A. 1976, ApJ, 208, 550

Pandharipande, V. R., & Smith, R. A. 1975, Nuclear Physics, Section A, 237, 507

Pechenick, K. R., Ftaclas, C., & Cohen, J. M. 1983, ApJ, 274, 846

Pethick, C. J., Ravenhall, D. G., Ventura, J., & Pines, D. 1991, Neutron Stars: Theory and Observation, 1st edn., NATO ASI Series 344 (Springer Netherlands), 33–34. http://gen.lib.rus.ec/book/index.php?md5=cc63a22a178906f0bd7c44921c586956

Potekhin, A. 2010, Physics Uspekhi, 53, 1235

Prakash, M., Lattimer, J. M., Pons, J. A., Steiner, A. W., & Reddy, S. 2001, Evolution of a Neutron Star from Its Birth to Old Age, ed. D. Blaschke, N. K. Glendenning, & A. Sedrakian, Vol. 578, 364

Rezzolla, L., Most, E. R., & Weih, L. R. 2018, ApJL, 852, L25

Rhoades, C. E., & Ruffini, R. 1974, Physical Review Letters, 32, 324

Ritter, H., & King, A. R. 2001, in Astronomical Society of the Pacific Conference Series, Vol. 229, Evolution of Binary and Multiple Star Systems, ed. P. Podsiadlowski, S. Rappaport, A. R. King, F. D'Antona, & L. Burderi, 423

Schutz, B. 2009, A First Course in General Relativity (Cambridge University Press), 251–270. https://books.google.ca/books?id=V1CGLi58W7wC

Shapiro, I. I. 1964, PRL, 13, 789

Shklovsky, I. S. 1967, ApJL, 148, L1

Sotani, H., & Miyamoto, U. 2018, PRD, 98, 044017

Stergioulas, N., & Friedman, J. L. 1995, ApJ, 444, 306

Walecka, J. 2017, Introduction to General Relativity: Solutions to Problems (World Scientific Publishing Company), 190,195,197. https://books.google.ca/books?id=blEyDwAAQBAJ

Watts, A. L., Andersson, N., Chakrabarty, D., et al. 2016, Reviews of Modern Physics, 88, 021001

Wijnands, R., & van der Klis, M. 1998, NAT, 394, 344

Wilson, J. R. 1974, PrL, 32, 849

Yagi, K., & Yunes, N. 2013, Science, 341, 365

Zeldovich, Y., & Novikov, I. 2014, Stars and Relativity, Dover Books on Physics (Dover Publications), 369,370. https://books.google.ca/books?id=69YIBAAAQBAJ

Zhou, X., Tong, H., Zhu, C., & Wang, N. 2017, MNRAS, 472, 2403